

Atmospheric neutrinos at Super-Kamiokande and parametric resonance in neutrino oscillations

E. Kh. Akhmedov^{1 *}, A. Dighe^{1 †}, P. Lipari², A. Yu. Smirnov^{1 ‡}

(1) *The Abdus Salam International Centre for Theoretical Physics, I-34100 Trieste, Italy*

(2) *University of Rome, “La Sapienza” and INFN, I-00185 Rome, Italy*

Abstract

We consider the oscillations of atmospheric neutrinos in the earth in the three-neutrino scheme with a Δm^2 hierarchy and a small admixture of the electron neutrino in the heavy mass eigenstate characterized by the mixing angle θ_{13} . We show that for $\Delta m^2 \simeq (0.5 - 3) \times 10^{-3} \text{ eV}^2$ indicated by the Super-Kamiokande data and $\sin^2 2\theta_{13} \lesssim 0.2$, the oscillations of multi-GeV neutrinos in the subdominant $\nu_\mu \leftrightarrow \nu_e$ mode are enhanced by the MSW and parametric resonances. The parametric resonance, which occurs when the neutrinos cross the core of the earth, dominates for $\Delta m^2 \simeq (1 - 2) \times 10^{-3} \text{ eV}^2$, $\sin^2 2\theta_{13} \lesssim 0.06$. The resonance matter effects lead to an observable excess of the e-like events with a specific zenith angle dependence even for small θ_{13} . The up-down asymmetry of the multi-GeV e-like events can reach 15% for $|\cos \Theta_e| > 0.2$ and up to 30% for $|\cos \Theta_e| > 0.6$, where Θ_e is the zenith angle of the electron. The resonance matter effects are relevant for the interpretation of the Super-Kamiokande data.

*On leave from National Research Centre Kurchatov Institute, Moscow 123182, Russia. E-mail: akhmedov@sissa.it

†E-mail: amol@ictp.trieste.it

‡Also at the Institute of Nuclear Research of Russian Academy of Sciences, Moscow 117312, Russia. E-mail: smirnov@ictp.trieste.it

1 Introduction

Neutrino oscillations in matter can be strongly enhanced if the matter density varies periodically along the neutrino path. In this case the parametric resonance of neutrino oscillations can occur [1, 2]. The probability of the transition of a neutrino from one flavor state to another may become close to unity even when the mixing angles (both in vacuum and in matter) are small. The parametric effects are further enhanced if the parametric resonance energy is close to that of the MSW resonance [3].

The simplest realization of the periodic matter density distribution, which in addition is of practical importance, is the periodic step function (“castle wall”) profile. In this case, the density modulation period L consists of two parts, L_c and L_m , which correspond to constant but different matter densities N_c and N_m . The evolution equation for neutrino oscillations in matter with such a density distribution allows for an exact analytic solution [2].

For the “castle wall” density profile, the parametric resonance conditions are especially simple: the lowest-order (principal) resonance occurs when the oscillation phases ϕ_m and ϕ_c defined through $\phi_i = 2\pi L_i/l_m(N_i)$ [$(i = m, c)$ with $l_m(N_i)$ being the oscillation length in the matter with density N_i] satisfy [2, 4]

$$\phi_c = \phi_m = \pi. \quad (1)$$

Recently it has been pointed out [4] that atmospheric neutrinos traversing the earth pass through layers of alternating density and can therefore undergo parametrically enhanced oscillations. Indeed, the earth consists of two main structures – the mantle and the core. The matter density changes rather slowly within the mantle and within the core but at their border it jumps sharply by about a factor of two. Therefore to a good approximation, one may consider the mantle and the core as structures of constant densities equal to the corresponding average densities (two-layer model)¹. Neutrinos coming to the detector from the lower hemisphere at zenith angles Θ_ν in the range defined by $\cos \Theta_\nu = (-1) \div (-0.837)$

¹A comparison of neutrino oscillation probabilities calculated with such a simplified matter density

traverse the earth's mantle, core and then again mantle. Therefore such neutrinos experience a periodic “castle wall” potential. Even though the neutrinos pass only through “one and a half” periods of density modulations (this would be exactly one and a half periods if the distances neutrinos travel in the mantle and core were equal), the parametric effects on neutrino oscillations in the earth can be quite strong [4, 6, 7].

In [4] the effect of parametric resonance on possible $\nu_\mu \leftrightarrow \nu_{sterile}$ oscillations of atmospheric neutrinos was considered. The effect was found to be potentially important for zenith angle distributions of through-going and stopping muons produced by high energy neutrinos. The parametric enhancement of atmospheric neutrino oscillations $\nu_\mu \leftrightarrow \nu_e$ was discovered numerically in [8]; however, in these papers the parametric nature of the enhancement was not recognized and possible consequences for atmospheric neutrino oscillations were not fully studied.

The parametric enhancement can also take place for oscillations of solar neutrinos in the earth. It was realized in [6, 7] that a sizeable enhancement of the regeneration effect for neutrinos crossing the core and having the energies lying between the MSW resonance energies in the core and in the mantle, found in [9], is due to the parametric resonance.

In the present paper we discuss in detail possible manifestations of the resonance matter effects and in particular, of the parametric resonance in *flavor* oscillations of atmospheric neutrinos. The Super-Kamiokande (SK) collaboration has recently reported a strong evidence for neutrino oscillations in their atmospheric neutrino data [10], confirming the previously observed anomaly in the flavor composition of atmospheric neutrinos [11].

The SK group has analyzed their data in the framework of two-flavor oscillations. They have shown that the data can be fitted well assuming $\nu_\mu \leftrightarrow \nu_\tau$ oscillations with the maximal or close to maximal mixing ($\sin^2 2\theta \simeq 1$) and $\Delta m^2 = (0.5 - 6) \times 10^{-3} \text{ eV}^2$. Pure $\nu_\mu \leftrightarrow \nu_e$ oscillations are practically excluded: they would have resulted in a significant zenith angle profile with those calculated with actual density profile provided by geophysical models shows a very good agreement (for recent discussions see, *e.g.*, [4, 5]).

dependence of the e-like events in contradiction with the observations. In addition, the sizeable deficiency of muon-like events would require a strong (close to maximal) $\nu_e - \nu_\mu$ mixing, which is excluded by the CHOOZ experiment [12] for most of the values of Δm^2 relevant for the atmospheric neutrino anomaly. At the same time, $\nu_\mu \leftrightarrow \nu_e$ oscillations with small mixing angles are still possible. Moreover, the data shows some excess of e-like events both in sub-GeV and multi-GeV samples and therefore is suggestive of the $\nu_\mu \leftrightarrow \nu_e$ oscillations as a subdominant mode. In the data analysis by the SK collaboration the excess of e-like events was accounted for by up-scaling the overall normalization of the fluxes of atmospheric neutrinos by factors which are compatible with the uncertainty of the theoretical predictions. However, recent cosmic ray measurements by the BESS experiment [13] indicate that the overall normalization of the atmospheric neutrino fluxes in the existing theoretical predictions was rather overestimated than underestimated. This makes the problem of the excess of e-like events more serious. In addition, the data, though not yet conclusive, seems to indicate some deviation of the zenith-angle dependence of the e-like events from the dependence that follows just from the zenith-angle dependence of the original flux in the absence of oscillations. Furthermore, it is difficult to explain the low value of the double ratio $R = (e/\mu)/(e/\mu)_{MC}$ in a wide range of neutrino energies just in terms of the $\nu_\mu \leftrightarrow \nu_\tau$ oscillations [14]. All this may indicate that the electron neutrinos are also involved in the oscillations.

In this paper we study the atmospheric neutrino oscillations in the 3-flavor scheme with $\nu_\mu \leftrightarrow \nu_\tau$ being the dominant channel. We assume that the vacuum $\nu_\mu - \nu_e$ mixing angle satisfies the upper bounds following from the CHOOZ data. We show that the MSW and parametric enhancements of atmospheric neutrino oscillations occur in the subdominant $\nu_\mu \leftrightarrow \nu_e$ mode, leading to observable effects despite the smallness of the mixing angle.

There have been a number of studies of the atmospheric neutrino oscillations with the three neutrino mixing [15, 16, 17, 18]. However, their authors have either concentrated on gross characteristics of the atmospheric neutrino oscillations (such as the allowed values

of mixing angles and mass squared differences) [15], or considered only the cases when all mixing angles are large and/or Δm_{atm}^2 is large [16], or employed the constant-density approximation of the structure of the earth [17], or neglected the matter effects on neutrino oscillations in the earth [18]. In the first case the results are rather insensitive to the parametric effects, while in the last three cases these effects are missed altogether.

Although the MSW enhancement effects are important and for a wide range of parameters dominate the excess of the multi-GeV e-like events, we concentrate here on the parametric resonance effects for two reasons: (1) in contrast to the MSW enhancement which was widely discussed in the past the parametric effects in the oscillations of atmospheric neutrinos have not been studied in detail; (2) the parametric resonance modifies the MSW resonance peaks.

The paper is organized as follows. In Sec. 2 we find the probabilities of oscillations in the three neutrino system in terms of the $\nu_e - \tilde{\nu}_3$ oscillation probability which experiences the resonance enhancement. In Sec. 3 we consider the parametric resonance effects on the atmospheric neutrinos. In Sec. 4 we present the results of the numerical calculations for the zenith angle dependence and the up-down asymmetry of the e-like and μ -like events and confront the results with observations. In Sec. 5 we discuss our results as well as the prospects of observing the parametric resonance in the oscillations of atmospheric neutrinos. The details of the calculations of the cross-sections and the event rates are given in the Appendix.

2 Three-flavor oscillations of atmospheric neutrinos

We consider the three-flavor neutrino system with a hierarchy of mass squared differences

$$\Delta m_{21}^2 \ll \Delta m_{32}^2 \approx \Delta m_{31}^2 . \quad (2)$$

We assume that $\Delta m_{32}^2 \equiv \Delta m_{atm}^2 \gtrsim 5 \times 10^{-4} \text{ eV}^2$ is relevant for the atmospheric neutrino oscillations whereas $\Delta m_{21}^2 \lesssim 10^{-5} \text{ eV}^2$ allows one to solve the solar neutrino problem either

through the MSW effect or through the long range vacuum oscillations.

The evolution of the neutrino vector of state $\nu_f \equiv (\nu_e, \nu_\mu, \nu_\tau)^T$ is described by the equation

$$i\frac{d\nu_f}{dt} = \left(\frac{UM^2U^\dagger}{2E} + V \right) \nu_f, \quad (3)$$

where E is the neutrino energy and $M^2 = \text{diag}(m_1^2, m_2^2, m_3^2)$ is the diagonal matrix of neutrino mass squared eigenvalues. $V = \text{diag}(V_e, 0, 0)$ is the matrix of matter-induced neutrino potentials with $V_e = \sqrt{2}G_F N_e$, G_F and N_e being the Fermi constant and the electron number density, respectively. The mixing matrix U , defined through $\nu_f = U\nu_m$ where $\nu_m = (\nu_1, \nu_2, \nu_3)^T$ is the vector of neutrino mass eigenstates, can be parametrized as

$$U = U_{23}U_{13}U_{12}. \quad (4)$$

The matrices $U_{ij} = U_{ij}(\theta_{ij})$ perform the rotation in the ij - plane by the angle θ_{ij} . We have neglected possible CP-violation effects in the lepton sector which are strongly suppressed in the case of the mass hierarchy (2).

Let us introduce new states $\tilde{\nu} = (\nu_e, \tilde{\nu}_2, \tilde{\nu}_3)^T$ obtained by performing the U_{23} - transformation: $\nu_f = U_{23}\tilde{\nu}$. The Hamiltonian \tilde{H} that describes the evolution of the $\tilde{\nu}$ state can be obtained from (3) and (4):

$$\tilde{H} = \frac{1}{2E} U_{13}U_{12}M^2U_{12}^\dagger U_{13}^\dagger + V.$$

We get explicitly

$$\tilde{H} \approx \begin{pmatrix} s_{13}^2 \Delta m_{32}^2 / 2E + V_e & 0 & s_{13}c_{13} \Delta m_{32}^2 / 2E \\ 0 & c_{12}^2 \Delta m_{21}^2 / 2E & 0 \\ s_{13}c_{13} \Delta m_{32}^2 / 2E & 0 & c_{13}^2 \Delta m_{32}^2 / 2E \end{pmatrix}, \quad (5)$$

($c_{13} \equiv \cos \theta_{13}$, $s_{13} \equiv \sin \theta_{13}$, etc.) after the following approximations. Since Δm_{32}^2 is in the range $\gtrsim 5 \times 10^{-4} \text{ eV}^2$ while $m_{21}^2 < 10^{-5} \text{ eV}^2$, the terms of the order $s_{12}^2 \Delta m_{21}^2 / \Delta m_{32}^2$ were neglected. Also, $s_{12}c_{12} \Delta m_{21}^2 / 2EV_e \lesssim 10^{-3}$, so the (12)-element in the matrix (5) (i.e. the mixing between the ν_e and $\tilde{\nu}_2$) was neglected.

According to (5), the $\tilde{\nu}_2$ state decouples from the rest of the system and evolves independently. Therefore the S-matrix (the matrix of amplitudes) in the basis $(\nu_e, \tilde{\nu}_2, \tilde{\nu}_3)$ has the following form :

$$S \approx \begin{pmatrix} A_{ee} & 0 & A_{e3} \\ 0 & A_{22} & 0 \\ A_{3e} & 0 & A_{33} \end{pmatrix}, \quad (6)$$

where

$$A_{22} = \exp(-i\phi_2), \quad \phi_2 = \frac{c_{12}^2 \Delta m_{21}^2 L}{2E}, \quad (7)$$

and L is the total distance traveled by the neutrinos. Notice that in our approximation ϕ_2 does not depend on the matter density. The $(\nu_e, \tilde{\nu}_3)$ subsystem evolves according to the 2×2 Hamiltonian [$\nu_e - \tilde{\nu}_3$ submatrix in (5)] determined by the potential V_e , mixing angle θ_{13} and the mass squared difference Δm_{32}^2 . Let us denote by

$$P_2 \equiv |A_{e3}|^2 = |A_{3e}|^2 = 1 - |A_{ee}|^2 = 1 - |A_{33}|^2 \quad (8)$$

the probability of the $\nu_e \leftrightarrow \tilde{\nu}_3$ oscillations. As we will show in Sec. 3, it is in this channel that the oscillations are parametrically enhanced.

The S -matrix in the flavor basis can be obtained from (6) by U_{23} rotation: $U_{23} S U_{23}^\dagger$. Then the probabilities of flavor oscillations in the three neutrino system can be found as $P(\nu_\alpha \rightarrow \nu_\beta) = |(U_{23} S U_{23}^\dagger)_{\alpha\beta}|^2$, which yields

$$P(\nu_e \rightarrow \nu_e) = 1 - P_2, \quad (9)$$

$$P(\nu_e \rightarrow \nu_\mu) = P(\nu_\mu \rightarrow \nu_e) = s_{23}^2 P_2, \quad (10)$$

$$P(\nu_e \rightarrow \nu_\tau) = c_{23}^2 P_2, \quad (11)$$

$$P(\nu_\mu \rightarrow \nu_\mu) = 1 - s_{23}^4 P_2 + 2s_{23}^2 c_{23}^2 \left[\text{Re}(e^{-i\phi_2} A_{33}) - 1 \right], \quad (12)$$

$$P(\nu_\mu \rightarrow \nu_\tau) = s_{23}^2 c_{23}^2 \left[2 - P_2 - 2\text{Re}(e^{-i\phi_2} A_{33}) \right]. \quad (13)$$

The phase ϕ_2 is defined in (7). The interpretation of the above results is straightforward. For instance, the $\nu_\mu \leftrightarrow \nu_e$ transition occurs via the projection of ν_μ onto $\tilde{\nu}_3$ and 2ν - oscillations

$\tilde{\nu}_3 \leftrightarrow \nu_e$. The $\nu_\mu \leftrightarrow \nu_\tau$ transition can occur in two different ways: (i) ν_μ projects onto $\tilde{\nu}_2$, the latter propagates without transition and at the final time of evolution is projected onto ν_τ ; (ii) ν_μ projects onto $\tilde{\nu}_3$; since $\tilde{\nu}_3$ oscillates into ν_e , at the final time one should project the amplitude of the survival probability of $\tilde{\nu}_3$ onto ν_τ . The interference of these two transition amplitudes leads to the probability (13).

Using the probabilities (9) - (13) one can find the modifications of the atmospheric neutrino fluxes due to the oscillations. Let F_e^0 and F_μ^0 be the electron and muon neutrino fluxes at the detector in the absence of oscillations. Then the fluxes in the presence of oscillations can be written as

$$F_e = F_e^0 [1 + P_2(rs_{23}^2 - 1)] \quad , \quad (14)$$

$$F_\mu = F_\mu^0 \left[1 - s_{23}^4 \left(1 - \frac{1}{rs_{23}^2} \right) P_2 + 2s_{23}^2 c_{23}^2 [Re(e^{-i\phi_2} A_{33}) - 1] \right] , \quad (15)$$

where

$$r(E, \Theta_\nu) = \frac{F_\mu^0(E, \Theta_\nu)}{F_e^0(E, \Theta_\nu)}$$

is the ratio of the original muon and electron neutrino fluxes.

It is interesting that one can have either an excess or a deficiency of e-like events depending on the values of r and s_{23} . Indeed, the effect of oscillations on the electron neutrino flux is proportional to the factor $(rs_{23}^2 - 1)$. If one assumes $r = 2$, there will be an excess of e-like events for $\theta_{23} > 45^\circ$ and a deficiency for $\theta_{23} < 45^\circ$. The SK best fit was $\theta_{23} = 45^\circ$; in this case there would be no deviation from the prediction for $r = 2$. However, for upward going neutrinos in the multi-GeV range r is typically 3 – 3.5 rather than 2, so there should be an excess of e-like events even if $\theta_{23} = 45^\circ$. In addition, notice that the SK analyses were performed in the two-flavor scheme, and the best-fit value of θ_{23} may be somewhat different in the 3-flavor analysis.

A final remark is that in the two neutrino mixing scenario, the probability of $\nu_\mu \leftrightarrow \nu_\tau$ oscillations depends on $\sin^2 2\theta_{23}$, and hence has an ambiguity $\theta_{23} \leftrightarrow (\pi/2 - \theta_{23})$. In the three

neutrino case the probability $P(\nu_e \leftrightarrow \nu_\mu)$ depends on s_{23}^2 , so that the study of an excess of the e-like events allows one to resolve the ambiguity.

3 Parametric enhancement of neutrino oscillations

The amplitude A_{33} and the probability P_2 which enter into the expressions (9) - (13) have to be found by solving the evolution equation for the $(\nu_e, \tilde{\nu}_3)$ system. The transitions in this system are the ones that undergo the resonance (parametric and MSW) enhancements. One can study properties of the resonance matter effects using the two-layer model of the earth's density profile. In the two-layer model P_2 and A_{33} can be found explicitly in a compact form [7]:

$$P_2 = \left(2 \sin \frac{\phi_m}{2} \sin 2\theta_m Y + \sin \frac{\phi_c}{2} \sin 2\theta_c \right)^2, \quad (16)$$

$$\begin{aligned} \text{Re}[e^{-i\phi_2} A_{33}] = & \left(2 \cos \frac{\phi_m}{2} Y - \cos \frac{\phi_c}{2} \right) \cos(\Phi - \phi_2) - \\ & \left(2 \sin \frac{\phi_m}{2} \cos 2\theta_m Y + \sin \frac{\phi_c}{2} \cos 2\theta_c \right) \sin(\Phi - \phi_2), \end{aligned} \quad (17)$$

where

$$Y \equiv \cos \frac{\phi_m}{2} \cos \frac{\phi_c}{2} - \sin \frac{\phi_m}{2} \sin \frac{\phi_c}{2} \cos(2\theta_m - 2\theta_c). \quad (18)$$

Here ϕ_m and ϕ_c are the oscillation phases acquired by the neutrino system in the mantle (one layer) and in the core, respectively. They can be written as

$$\phi_i = \frac{2\pi L_i}{l_m(V_i)} = L_i \Delta H(V_i), \quad (i = m, c), \quad (19)$$

where

$$\Delta H(V_i) = \sqrt{\left(\cos 2\theta_{13} \frac{\Delta m_{32}^2}{2E} - V_i \right)^2 + \left(\sin 2\theta_{13} \frac{\Delta m_{32}^2}{2E} \right)^2} \quad (20)$$

is the level splitting (difference between the eigenvalues of H), V_m and V_c being the potentials in the mantle and in the core. The angles θ_m and θ_c are the values of the $\nu_e - \tilde{\nu}_3$ mixing

angle in matter of the mantle and the core respectively. They can be found from

$$\sin 2\theta_i = \sin 2\theta_{13} \frac{\Delta m_{32}^2}{2E\Delta H(V_i)}, \quad (i = m, c). \quad (21)$$

The phase Φ is given by the integral of $(\Delta m_{32}^2/4E + V_e/2)$ along the neutrino path between its production and detection points. In the two-layer model of the earth's density profile, it is given by

$$\Phi = \left(\frac{\Delta m_{32}^2}{2E} + V_m \right) L_m + \left(\frac{\Delta m_{32}^2}{2E} + V_c \right) \frac{L_c}{2} \quad (22)$$

(we neglect the neutrino oscillations in the air which are unimportant for the range of the neutrino parameters of interest). For neutrinos crossing both the core and the mantle ($\sin^2 \Theta_\nu < (R_c/R_\oplus)^2 = 0.299$) the path lengths in the mantle and the core are determined by the relations

$$L_m = R_\oplus \left(-\cos \Theta_\nu - \sqrt{(R_c/R_\oplus)^2 - \sin^2 \Theta_\nu} \right), \quad (23)$$

$$L_c = 2R_\oplus \sqrt{(R_c/R_\oplus)^2 - \sin^2 \Theta_\nu}. \quad (24)$$

Here R_\oplus is the radius of the earth and R_c is the radius of the core. For $\sin^2 \Theta_\nu \geq 0.299$ neutrinos cross the mantle only and their path length is $2L_m = -2R_\oplus \cos \Theta_\nu$.

The physical picture of the oscillations and the resulting event rates depend crucially on the neutrino parameters Δm_{32}^2 and $\sin^2 2\theta_{13}$ as well as on the zenith angle Θ_ν . Let us consider the dependence of the oscillation probability on the neutrino energy. In the region

$$\frac{E}{\Delta m_{32}^2} = (0.8 - 4) \cdot 10^{12} \text{ eV}^{-1} \quad (25)$$

neutrinos experience resonantly enhanced oscillations in matter. This interval is determined by the MSW resonance energies for oscillations in the core and in the mantle E_c^R and E_m^R

$$E_i^R = \frac{\Delta m_{32}^2 \cos 2\theta_{13}}{2V_i} \quad (i = c, m) \quad (26)$$

and by the resonance widths $\Delta E/E_i^R \sim 2 \tan 2\theta_{13}$. The MSW resonance enhancement leads to characteristic peaks in the energy dependence of the transition probability. The exact positions of the maxima of the peaks depend on the oscillation phases and in general

do not coincide with the resonance energies (26). Neutrinos having the trajectories with $\cos \Theta_\nu > -0.84$ do not cross the core of the earth and therefore for such neutrinos only the MSW resonance enhancement of the oscillations in the mantle can occur.

For $\cos \Theta_\nu < -0.84$ there is an interference between the oscillation effects in the core and in the mantle which strongly depends on $\sin 2\theta_{13}$. For $\sin^2 2\theta_{13} > 0.15$ there is a significant overlap of the MSW resonances in the core and in the mantle. The interference leads to a rather complicated picture of neutrino oscillations in the overlap region with a modification of the MSW resonance peaks. The parametric resonance conditions are not fulfilled.

For $\sin^2 2\theta_{13} < 0.15$ the probability P_2 as a function of E has three main peaks: two peaks with the maxima at $\sim E_c^R$ and $\sim E_m^R$ due to the MSW resonance oscillations in the core and the mantle respectively, and a peak between them (fig. 1a). The latter is due to the parametric enhancement of oscillations. In what follows we shall call for brevity the resonance peaks due to the MSW effects for neutrinos oscillations in the earth' mantle and core *the mantle peak* and *the core peak* respectively.

The maximum of the parametric peak is at an energy E_p at which the resonance conditions (1) are satisfied; the analysis [6, 7] of the parametric resonance condition shows that a significant parametric enhancement occurs only when

$$\frac{E}{\Delta m_{32}^2} \simeq (1 - 2) \cdot 10^{12} \text{ eV}^{-1}, \quad (27)$$

i.e. E_p is indeed in the range $E_c^R < E_p < E_m^R$.

At the maximum of the parametric peak the transition probability (16) takes the value [4]

$$P_2^{max} = \sin^2 2(\theta_c - 2\theta_m) \quad (28)$$

provided that the resonance conditions are exactly fulfilled. Due to a small number of periods ("1.5 period"), the energy width of the parametric resonance $\Delta E/E_p$ is large. The transition probability decreases by a factor of two for [7]

$$\Delta\phi_i = |\phi_i - \pi| \simeq \frac{\pi}{2}, \quad (i = c, m). \quad (29)$$

Thus, the resonance enhancement of neutrino oscillations can occur even for quite sizeable detuning of the phases $\phi_{m,c}$. Numerically we get $\Delta E/E_p \sim 2 - 3$.

Let us stress that the interference of the mantle and the core oscillation effects leads not only to the appearance of the parametric peak. It also modifies significantly the MSW peaks as compared with the peaks which would appear in the one layer cases without interference. In fact, the interference leads to a suppression of those peaks.

The parametric resonance conditions (1) constrain the allowed values of θ_{13} . If these conditions are to be satisfied for all the neutrino trajectories that cross the core (including the vertical ones) one gets from (1) the upper limit $\sin^2 2\theta_{13} \leq \pi^2 / (4(L_c)_{max}^2 V_c^2) \simeq 0.04$ [7]. If the zenith angles close to 180° are excluded, the constraint becomes less stringent. For example, for $\sin^2 \Theta_\nu \geq 0.12$ one obtains $\sin^2 2\theta_{13} \leq 0.07$.

The main features of the parametric peak are illustrated in fig. 1. For $\cos \Theta_\nu \simeq -1$ the parametric peak and the core peak partially overlap (actually the core peak appears as a shoulder on the low-energy slope of the parametric peak). With increasing $\cos \Theta_\nu$ the parametric peak moves towards larger energies; it becomes well resolved from the MSW peaks in the interval $\cos \Theta_\nu = (-0.94) \div (-0.87)$ and eventually transforms into the mantle peak at $\cos \Theta_\nu > -0.85$.

The relative strength (area) of the parametric and the MSW peaks depends on the value of θ_{13} . As follows from fig. 1b, with decreasing θ_{13} the MSW peaks decrease faster than the parametric peak. This can be explained as follows. For a given value of θ_{13} and Θ_ν there is in general some detuning at the parametric peak, i.e. the conditions (1) are only approximately satisfied. With decreasing $\sin^2 2\theta_{13}$ the maximal possible value (28) of the probability P_2 , which corresponds to the exact parametric resonance, decreases. At the same time, it turns out that the detuning becomes smaller which partially compensates the decrease in P_2^{max} . Therefore in some range of θ_{13} the parametric peak lowers only moderately with decreasing $\sin^2 2\theta_{13}$. In contrast to this, the MSW peaks decrease rather quickly with $\sin^2 2\theta_{13}$. As a result, for $\sin^2 2\theta_{13} < 0.06$ the parametric peak has the largest strength.

To summarize, the parametric peak is the most pronounced in the ranges of the parameters characterized by eq. (27) and

$$\sin^2 2\theta_{13} = (1 - 12) \cdot 10^{-2}, \quad \cos \Theta_\nu = (-1) \div (-0.84). \quad (30)$$

For the sub-GeV sample of e-like and μ -like events the relevant energies of neutrinos are $E \approx 0.3 - 1.5$ GeV. Then from (27) we find that for the sub-GeV events a significant effect of the parametric resonance is expected if the mass squared difference is in the range

$$\Delta m_{32}^2 \approx (1 - 10) \cdot 10^{-4} \text{ eV}^2. \quad (31)$$

The multi-GeV sample gets its main contribution from neutrinos with energies $E \approx 1.3 - 10$ GeV and the corresponding Δm_{32}^2 are larger:

$$\Delta m_{32}^2 = (0.4 - 4) \cdot 10^{-3} \text{ eV}^2. \quad (32)$$

Quite interestingly, the central value of this range coincides with the best fit value of Δm_{32}^2 which follows from the analysis of the contained events in SK [10].

The parametric resonance can play an important role for certain samples of events (*e.g.* multi-GeV) which pick up a relatively narrow neutrino energy interval. The number of events is determined by the integral over neutrino energy E of the oscillation probability folded in with the response function $f(E)$: $N \propto \int dE f(E) P(E)$. The response function describes the contribution of neutrinos with energy E to a given sample of events. In particular, the response function for the multi-GeV events in the Super-Kamiokande has a maximum at $E \approx 2.5$ GeV. The value of f increases rapidly with energy below the maximum but has a rather long tail above it; the energies at the half-height are $E \simeq 1.5$ and 4 GeV. Thus the width of the response function is characterized by a factor of 2 - 3.

As can be seen from fig. 1, for $\Delta m_{32}^2 \simeq (1.5 - 2) \times 10^{-3} \text{ eV}^2$ and values of $\cos \Theta_\nu$ varying in the range $(-1) \div (-0.84)$ (i.e. covering the earth's core), the parametric peak spans essentially the whole region of energies that corresponds to the peak of the response function of multi-GeV neutrinos. effect in the core). The mantle peak is in the tail of the

response function and therefore its contribution to the excess of e-like events is attenuated. For $\sin^2 2\theta_{13} < 0.06$ the contribution of the parametric peak dominates for trajectories crossing the core of the earth. However, even for higher values of θ_{13} ($\sin^2 2\theta_{13} \lesssim 0.15$) the contribution of the parametric resonance to the excess of e-like events can be comparable to that of the mantle and core peaks provided that $\Delta m_{32}^2 \sim (1 - 2) \times 10^{-3} \text{ eV}^2$.

For $\Delta m_{32}^2 \lesssim 10^{-3} \text{ eV}^2$ the overlap of the parametric peak and the peak of the response function is small and the main contribution to the excess of e-like events comes from the mantle peak.

For $\Delta m_{32}^2 > (2 - 3) \times 10^{-3} \text{ eV}^2$, with increasing Δm_{32}^2 the resonance effects weaken and the oscillation effects are essentially reduced to those of vacuum oscillations.

4 Resonance effects and zenith angle dependence of e-like and μ -like events

The resonance matter effects in the atmospheric neutrino oscillations can manifest themselves as an enhanced excess of the e-like events with a specific zenith angle dependence. We calculate the zenith angle distributions of the e-like and μ -like events for $\Delta m_{32}^2 = (0.1 - 10) \times 10^{-3} \text{ eV}^2$, $\sin^2 2\theta_{23} \gtrsim 0.7$ indicated by the SK data and a wide range of values of $\sin^2 2\theta_{13}$ taking the CHOOZ bounds into account. We examine whether the matter effects, and in particular the parametric resonance, can be relevant for understanding such features of the SK data as the excess of the e-like events and the asymmetries of e-like and μ -like events.

The number of e-like or μ -like events with the detected charged lepton in the energy interval ΔE_l and direction Ω_l ($l = e, \mu$) can be calculated as

$$N_l(\Omega_l) = \sum_{\nu, \bar{\nu}} \int_{\Delta E_l} dE_l \int d\Omega_{\nu l} \int d\Omega_{\nu} \int dE_{\nu} F_l(E_{\nu}, \Omega_{\nu}) \times$$

$$\frac{d^2\sigma(E_\nu, E_l, \Omega_{\nu l})}{dE_l d\Omega_{\nu l}} \delta[\Omega_l - (\Omega_\nu \oplus \Omega_{\nu l})] \epsilon(E_l) , \quad (33)$$

where $F_l(E_\nu, \Omega_\nu)$, ($l = e, \mu$) are the fluxes of neutrinos in the detector defined in eqs. (14), (15); E_l is the energy of the charged lepton. Up to the small geomagnetic effects the neutrino fluxes and therefore the charged lepton distributions depend only on the zenith angle: $N_l(\cos \Theta_l) = 2\pi N_l(\Omega_l)$. $\Omega_{\nu l}$ is the angle between the directions of the incoming neutrino and the outgoing lepton, $d^2\sigma/dE_l d\Omega_{\nu l}$ is the neutrino charged current cross-section, $\epsilon(E_l)$ is the charged lepton detection efficiency, and the integration goes over $E_l > 1.3$ GeV ($E_l < 1.3$ GeV) for multi-GeV (sub-GeV) sample.

In calculating the neutrino fluxes at the detector we have used the two-layer model of the earth's structure [eqs. (16) - (24)]; the average densities of the core and the mantle were calculated for each neutrino trajectory using the actual density profile provided by the Stacey model [19]. For $\Delta m_{21}^2 < 10^{-5}$ eV² the correction due to the phase ϕ_2 in eq. (15) is very small, and we have put $\phi_2 = 0$ in the actual calculations. The details of the calculations of the cross-sections and the decay rates are described in the Appendix.

The integration over the neutrino zenith angles and energies leads to a significant smearing of the Θ_l dependence. Indeed, the average angle between the neutrino and the outgoing charged lepton is about $15^\circ - 20^\circ$ in the multi-GeV region and it is almost 60° in the sub-GeV range. Therefore the data do not give us direct information about the zenith angle dependence of ν_e and ν_μ fluxes at the detector. In particular, a significant contribution to the vertical upward bin $\cos \Theta_l = (-1 \div -0.8)$ comes from the neutrinos which cross the mantle only and therefore do not experience the parametric enhancement of oscillations. Thus, the observed parametric enhancement effects are weakened as compared to the enhancement in the neutrino zenith angle distributions. This is especially true for the sub-GeV sample. Additional smearing of the neutrino zenith angle dependence due to the finite angular and energy resolution is relatively small.

In the antineutrino channels, matter suppresses oscillations² and consequently the parametric effects are weak. Since neutrinos and antineutrinos of a given flavor are not distinguished in the atmospheric neutrino experiments (*i.e.* only total $\nu_e + \bar{\nu}_e$ and $\nu_\mu + \bar{\nu}_\mu$ fluxes are measured), the resonance enhancement effects are additionally diluted.

Let us first consider the multi-GeV events. In Fig. 2 we show the zenith angle dependences of the e-like and μ -like events for a representative set of the oscillation parameters Δm_{32}^2 , $\sin^2 2\theta_{13}$ and $\sin^2 \theta_{23}$. The e-like events exhibit an excess which first appears in the horizontal bin ($\cos \Theta_e \simeq 0$) and increases monotonically with decreasing $\cos \Theta_e$. It reaches $\sim 20\%$ in the vertical (upward) bin, $\cos \Theta_e \simeq -1$. In contrast to this, μ -like events exhibit a deficiency at $\cos \Theta_\mu < 0$.

A convenient quantitative measure of the excess or deficiency of e-like and μ -like events in the vertical bins is the up-down asymmetry

$$A_l^{U/D}(b_1, b_2) = 2 \frac{N_l^{up}(b_1, b_2) - N_l^{down}(b_1, b_2)}{N_l^{up}(b_1, b_2) + N_l^{down}(b_1, b_2)}, \quad (l = e, \mu), \quad (34)$$

where

$$N_l^{up}(b_1, b_2) = \int_{-b_2}^{-b_1} d \cos \Theta_l N_l(\Theta_l), \quad N_l^{down}(b_1, b_2) = \int_{b_1}^{b_2} d \cos \Theta_l N_l(\Theta_l), \quad (35)$$

and $N_l(\cos \Theta_l)$ are given in (33). The parametric as well as the MSW resonance enhancement effects are largest in the vertical (upward) bins. In most of our calculations we use $b_1 = 0.6$, $b_2 = 1$ which corresponds to the SK binning. Notice that about 60% of neutrinos contributing to this bin have the trajectories which cross the mantle only and therefore do not undergo the parametric enhancement of oscillations.

From the SK results [10] we find

$$A_e^{U/D}(0.6, 1) \approx 0.22 \pm 0.21. \quad (36)$$

The up-down asymmetry and the excess of the e-like events increase with increasing s_{23}^2 . In order to assess the maximal possible effects we therefore choose for most of our calculation the value $s_{23}^2 = 0.75$ which is close to the upper border of the values allowed by the SK data.

²We assume $\Delta m_{32}^2 > 0$ throughout the paper.

In fig. 3a we show the dependence of the up-down asymmetry $A_e^{U/D}(0.6, 1)$ on Δm_{32}^2 for $s_{23}^2 = 0.75$ and different values of $\sin^2 2\theta_{13}$. The dependence of $A_e^{U/D}$ on Δm_{32}^2 reflects the changing degree of overlap of the response function with the parametric peak as well as the MSW peaks (see Sec. 3). The maximum of the asymmetry ($A_e^{U/D}(0.6, 1) \simeq 0.15 - 0.25$) is at $\Delta m_{32}^2 \approx (0.8 - 2) \times 10^{-3} \text{ eV}^2$. Thus, our calculations for $\sin^2 2\theta_{13} \gtrsim 0.06$ reproduce the central value of the up-down asymmetry observed by the SK (36). They also reproduce (within 1σ) the experimentally observed excess of e-like events in the vertical bin.

With decreasing $\sin^2 2\theta_{13}$ the asymmetry decreases and the maximum shifts to larger values of Δm^2 . Indeed, for large θ_{13} ($\sin^2 2\theta_{13} \sim 0.1$) the mantle peak gives the main contribution and the maximum of asymmetry at $\Delta m_{32}^2 = 0.8 \times 10^{-3} \text{ eV}^2$ reflects the position of this peak. With decreasing θ_{13} the parametric peak becomes relatively more important and the maximum of asymmetry shifts to $\Delta m_{32}^2 \approx (1.5 - 1.7) \times 10^{-3} \text{ eV}^2$ at $\sin^2 2\theta_{13} \sim 0.06$, which corresponds to the position of the parametric peak. With further decrease of θ_{13} the position of the maximum remains unchanged, in accordance with fig. 1b. We find that for $\sin^2 2\theta_{13} \sim 0.025$ the contribution of the parametric peak to the excess of the e-like events is about 60%.

With decreasing Δm_{32}^2 the asymmetry decreases since the mixing in matter (and consequently the oscillation probability) decreases. For $\Delta m_{32}^2 < 0.3 \times 10^{-3} \text{ eV}^2$ it approaches the asymmetry due to the geomagnetic effect without oscillations.

For $\Delta m_{32}^2 > 3 \times 10^{-3} \text{ eV}^2$ the asymmetry decreases with increasing Δm_{32}^2 for two reasons. (i) The matter enhancement of mixing disappears and the oscillation effect is essentially reduced to that of *vacuum* oscillations governed by the small $\sin^2 2\theta_{13}$ (the oscillations due to the matter splitting between the levels of the two light eigenstates are suppressed by the factor $\sin^2 2\theta_{13} \cdot \sin^2 2\theta_{23}/4$ [17]); (ii) for $\Delta m_{32}^2 \gtrsim 5 \times 10^{-2} \text{ eV}^2$ the oscillations become important for down-going neutrinos too and the up-down asymmetry goes to zero.

In fig. 3b we show the asymmetry of μ -like events, which is opposite in sign to that for the e-like events. The absolute value of the asymmetry becomes maximal at $\Delta m_{32}^2 \sim 0.3 \times 10^{-3}$

eV^2 . This corresponds to the situation when the average distance in the vertical bin ($\sim 10^4$ km) equals half of the vacuum oscillation length for a typical energy of multi-GeV neutrinos $E \sim 2$ GeV. The matter effects are important in the range $\Delta m_{32}^2 \sim (0.5 - 5) \times 10^{-3} \text{ eV}^2$ where the absolute value of the asymmetry increases with $\sin^2 2\theta_{13}$ just as in fig. 3a. We show by dotted line the asymmetry which would be expected in the case of pure $\nu_\mu \leftrightarrow \nu_\tau$ oscillations with the same $s_{23}^2 = 0.75$. (For $2 \times 10^{-3} \lesssim \Delta m_{32}^2/\text{eV}^2 \lesssim 10^{-2}$ it can be roughly estimated assuming that in this range the oscillations of upward going neutrinos are fully averaged whereas the downward going neutrinos do not oscillate at all, which yields $A_\mu^{U/D} \approx \sin^2 2\theta_{23}/(2 - 0.5 \sin^2 2\theta_{23}) = -0.46$.) The difference between the dotted line and the others shows the enhancement of the asymmetry due to an additional channel of oscillations $\nu_\mu \leftrightarrow \nu_e$ in the three neutrino system. In the case of $\nu_\mu \leftrightarrow \nu_\tau$ oscillations with maximal mixing the asymmetry is larger: $A_\mu^{U/D} \sim -0.67$. Both values are compatible with the SK result, -0.56 ± 0.15 [10].

As we have pointed out above, the parametric enhancement of neutrino oscillations occurs for neutrinos crossing the earth's core ($\cos \Theta_\nu < -0.84$). Therefore the largest up-down asymmetry is achieved when the binning enhances the contribution of the core-crossing neutrinos. In fig. 3c we compare the electron asymmetries in the bins $0.84 \leq |\cos \Theta_{\nu_e}| \leq 1$, $0.60 \leq |\cos \Theta_{\nu_e}| \leq 0.84$ and $0.60 \leq |\cos \Theta_{\nu_e}| \leq 1$. One can see that the asymmetry is largest for the first bin which has the maximal contribution from the neutrinos crossing the core of the earth. The maximum of asymmetry is achieved at $\Delta m_{32}^2 \simeq (1.5 - 1.7) \times 10^{-3} \text{ eV}^2$ which is typical of the parametric resonance at multi-GeV energies. The position of the peak of the asymmetry in the second bin which is dominated by the mantle-only crossing neutrinos ($\Delta m_{32}^2 \simeq 0.7 \times 10^{-3} \text{ eV}^2$) reflects the position of the MSW peak in the mantle. The parametric peak is higher than the MSW one because for small $\sin^2 2\theta_{13}$ the parametric effects dominate. In the third (largest) bin, $0.60 \leq |\cos \Theta_{\nu_e}| \leq 0.84$, the parametric effects are significantly diluted compared to the first bin.

To summarize, the physical picture of the neutrino oscillations depends crucially on the

value of Δm_{32}^2 . The whole range of Δm_{32}^2 can be divided into three parts:

- (1) the region of the vacuum oscillations: $\Delta m_{32}^2 \gtrsim 3 \times 10^{-3} \text{ eV}^2$ for multi-GeV neutrinos (here there is also a small effect due to the matter-induced level splitting of the light states);
- (2) the resonance region (two MSW resonances and the parametric resonance): $\Delta m_{32}^2 \simeq (0.5 - 3) \times 10^{-3} \text{ eV}^2$;
- (3) the region of matter suppressed oscillations $\Delta m_{32}^2 \lesssim 0.5 \times 10^{-3} \text{ eV}^2$.

For sub-GeV neutrinos the corresponding regions are shifted by about a factor of 3 to smaller values of Δm_{32}^2 .

In fig. 4a, we show the dependence of the up-down asymmetry $A^{U/D}(0.6, 1)$ on $\sin^2 2\theta_{13}$ for $s_{23}^2 = 0.75$ and several values of Δm_{32}^2 . The dashed curve corresponds to the value $\Delta m_{32}^2 = 1.7 \times 10^{-3} \text{ eV}^2$ from the resonance region. The asymmetry (and the excess) of the e-like events rapidly increases with $\sin^2 2\theta_{13}$ in the region $\sin^2 2\theta_{13} \lesssim 0.10$ which corresponds to the parametric resonance, and then increases more slowly.

The solid line corresponds to a value of Δm_{32}^2 close to the vacuum oscillation region. For $\sin^2 2\theta_{13} > 0.08$ the asymmetry increases almost linearly with $\sin^2 2\theta_{13}$, as is expected in the case of vacuum oscillations. Here, too, the CHOOZ bound is important: for the allowed values ($\sin^2 2\theta_{13} < 0.16$) the asymmetry is smaller than that for the value $\Delta m_{32}^2 = 1.7 \times 10^{-3} \text{ eV}^2$ from the resonance region. The dot-dashed line represents the asymmetry in the region of the matter suppressed oscillations: the effective mixing is suppressed even for large $\sin^2 2\theta_{13}$ and the asymmetry is relatively small. In fig. 4b, we show the corresponding asymmetry in the μ -like events.

As follows from (14), the asymmetry in the e-like events is proportional to the factor $(\bar{r}s_{23}^2 - 1)$, where $\bar{r} \sim 2.5$ is the ratio of the original muon and electron neutrino fluxes averaged over the zenith angles and energies in the multi-GeV sample. According to this, the asymmetry due to the oscillations increases almost linearly with s_{23}^2 (fig. 5a); it becomes zero at $s_{23}^2 \sim \bar{r}^{-1} \sim 0.4$, where the total asymmetry, $A \sim 0.05$, equals the small asymmetry due to the geomagnetic effects.

In fig. 5b, we show the dependence of the up-down asymmetry for μ -like events on s_{23}^2 . For pure $\nu_\mu \leftrightarrow \nu_\tau$ vacuum oscillations (dotted curve), the up-down asymmetry is a symmetric function with respect to $s_{23}^2 \leftrightarrow (1 - s_{23}^2)$. Matter effects break this symmetry and the breaking increases with s_{23}^2 in accordance with our previous analysis.

With increasing s_{23}^2 the excess of the e-like events gets enhanced. At the same time, for $\theta_{23} > 45^\circ$, the probability of the $\nu_\mu \leftrightarrow \nu_\tau$ oscillations decreases with increasing s_{23}^2 . The additional channel of oscillations $\nu_\mu \leftrightarrow \nu_e$ does not compensate for this decrease, and so the asymmetry and the total suppression of the μ - like events become smaller (see fig. 5 a, b).

The zenith angle dependence of the multi-GeV e-like events with and without $\nu_e \leftrightarrow \nu_\mu$ oscillations is shown in fig. 6, along with the SK data for 535 days. One can see that taking into account the $\nu_e \leftrightarrow \nu_\mu$ oscillations improves the fit of the data but cannot fully explain the excess of the e-like events unless the overall normalization of the atmospheric ν_e and ν_μ fluxes is increased.

In fig. 7 the iso-asymmetry curves for multi-GeV e-like events are plotted in the $(\sin^2 2\theta_{13}, \Delta m_{32}^2)$ plane, along with the constraints from the CHOOZ experiment (shaded area). The behavior of the curves can be understood from the preceding discussion. The large- Δm_{32}^2 region of the plot corresponds to the vacuum oscillations; vertical and near-vertical lines are due to the averaged oscillations with no or little dependence of probability on Δm_{32}^2 . Matter effects increase the asymmetry in the region $\Delta m_{32}^2 \simeq (0.5 - 3) \times 10^{-3} \text{ eV}^2$: the iso-asymmetry curves are “pulled” towards the region of small values of $\sin^2 2\theta_{13}$. For $\Delta m_{32}^2 \lesssim 0.5 \times 10^{-3} \text{ eV}^2$ matter suppresses the $\nu_e \leftrightarrow \nu_\mu$ oscillations.

The parameter space of the resonance region can be divided into three parts: (i) $\Delta m_{32}^2 \lesssim 10^{-3} \text{ eV}^2$, where the mantle resonance dominates; (ii) $\Delta m_{32}^2 \gtrsim 1.5 \times 10^{-3} \text{ eV}^2$, $\sin^2 2\theta_{13} < 0.06$, where the parametric resonance gives an important contribution; (iii) $\Delta m_{32}^2 \gtrsim 1.5 \times 10^{-3} \text{ eV}^2$, $\sin^2 2\theta_{13} \simeq 0.06 - 0.12$, where parametric peak gives a smaller contribution which, however, is comparable to that due to the mantle resonance. The core resonance gives a smaller effect.

For $\sin^2 2\theta_{13} > 0.15$ there is a complex interference of the MSW resonance effects in the mantle and core.

The CHOOZ bound excludes the part of the parameter space that corresponds to large asymmetry, $A_e^{U/D}(0.6, 1) > 0.28$. There is a local maximum of the asymmetry $A_e^{U/D}(0.6, 1) \simeq 0.27$ at $\sin^2 2\theta_{13} \simeq 0.14$, $\Delta m_{32}^2 \simeq 10^{-3} \text{ eV}^2$. Values close to this can also be achieved at the same $\Delta m_{32}^2 \simeq 10^{-3} \text{ eV}^2$ but large mixing angles $\sin^2 2\theta_{13} \simeq 0.5 - 0.9$. From fig. 7 it follows that the asymmetry $A_e^{U/D}(0.6, 1)$ can be as large as 0.22 in the range of parameters (ii), i.e. rather close to the maximal possible value indicated above.

The parametric enhancement of the $\nu_e \leftrightarrow \nu_\mu$ oscillations makes it possible to have a sizeable asymmetry even for very small values of the mixing angle θ_{13} : the asymmetry can be as large as 0.15 even for $\sin^2 2\theta_{13} = 0.02$ provided that Δm_{32}^2 lies in the range $(1-2) \times 10^{-3} \text{ eV}^2$. Notice that in the absence of matter effects one would expect the asymmetry to be an order of magnitude smaller.

The iso-asymmetry plot of fig. 7 has been obtained for the fixed value of s_{23}^2 ($s_{23}^2 = 0.75$); the magnitudes of the asymmetry for other values of s_{23}^2 can be easily found using the relation $A_e^{U/D} = 2x/(2+x)$, where $x = (s_{23}^2 \bar{r} - 1)P_2$.

As we have pointed out above, the largest asymmetry allowed by the CHOOZ constraints, $A_e^{U/D}(0.6, 1) \simeq 0.28$, is achieved in a small region around $\Delta m_{32}^2 \simeq 0.8 \times 10^{-3} \text{ eV}^2$ and $\sin^2 2\theta_{13} \simeq 1$ (see fig. 7). Future reactor experiments, and in particular KAMLAND [20], will be able to probe this range of parameters. If no oscillations are found, the values $\sin^2 2\theta_{13} \geq 0.1$ will be excluded. In this case the largest possible asymmetry would correspond to the small- θ_{13} region where the parametric resonance effects play an important role. It should also be emphasized that in case of the negative result of KAMLAND the studies of the excess of the e-like events in atmospheric neutrinos would be a unique way to probe the parameter range $\sin^2 2\theta_{13} < 0.1$, $\Delta m_{32}^2 > 5 \times 10^{-4} \text{ eV}^2$.

The calculated event rates are sensitive to the response function used. The latter depends on the event selection criteria, detection efficiency and other features of detector,

etc.. The results given above correspond to the response function described in Sec. 3. The response function with the maximum (and median energy) shifted by about 25% to higher energies compared to what we used would shift the iso-asymmetry contours by about 25% to larger Δm^2 . Notice that in this case the region of large asymmetries at large mixing angles will be completely excluded and the largest asymmetry would be achieved at $\sin^2 2\theta_{13} \sim 0.15$.

Let us now consider possible effects in the sub-GeV sample. In fig. 8 we show the zenith angle dependence of the sub-GeV events for $\Delta m_{32}^2 = 0.3 \times 10^{-3} \text{ eV}^2$ which corresponds to the maximum of the resonance effects. Due to the strong smearing, the excess has a rather weak zenith angle dependence. Moreover, even in the vertical bin it does not exceed 10%. The up-down asymmetry is smaller than 0.03. Notice that in the sub-GeV region \bar{r} is closer to 2 than in the multi-GeV region and the factor $\bar{r}s_{23}^2 - 1$ in (14) leads to an additional suppression of the transition probability.

In fig. 9a we show the dependence of ratio N_e/N_e^0 of the total numbers of the sub-GeV events on Δm_{32}^2 with and without oscillations. The matter oscillations enhance the excess of e-like events in the range $\Delta m_{32}^2 = (0.1 - 1) \times 10^{-3} \text{ eV}^2$ and the maximum is at $\Delta m_{32}^2 \simeq 0.3 \times 10^{-3} \text{ eV}^2$.

For $\Delta m_{32}^2 > 10^{-3} \text{ eV}^2$, which corresponds to the maximal effect in the multi-GeV sample, the oscillation effect in the sub-GeV sample approaches that of the vacuum oscillations. For $\sin^2 2\theta_{13} < 0.1$, we find that the total excess of the e-like events is below 5% and the asymmetry is below 3%.

The ratio N_μ/N_μ^0 is mainly determined by the $\nu_\mu \rightarrow \nu_\tau$ oscillations. In the 2-flavor case ($\theta_{13} = 0$) these oscillations are unaffected by matter. Therefore in the 3-flavor case for small values of θ_{13} the matter effects on N_μ/N_μ^0 are relatively small (fig. 9b).

5 Discussion and conclusions

The excess of e-like events both in multi-GeV and sub-GeV samples observed by the SK experiment may indicate that the electron neutrinos are involved in the oscillations of atmospheric neutrinos. In this connection we have considered the oscillations of atmospheric neutrinos in the 3ν scheme. Assuming the mass hierarchy $\Delta m_{32}^2 \approx \Delta m_{31}^2 \gg \Delta m_{21}^2$ we have derived simple analytic expressions for the oscillation probabilities in the 3ν system in terms of the oscillation amplitudes in the 2ν system $(\nu_e, \tilde{\nu}_3)$, where $\tilde{\nu}_3$ is a linear combination of ν_μ and ν_τ . For the amplitudes of the $\nu_e \leftrightarrow \tilde{\nu}_3$ oscillations in the earth analytic expressions obtained in the two-layer model of the earth's structure were used.

Let us summarize our main results. We have shown that the range of the neutrino parameters $\sin^2 2\theta_{13} \lesssim 0.2$, $\Delta m_{32}^2 \approx (0.5 - 3) \times 10^{-3} \text{ eV}^2$ is the resonance range for multi-GeV events in which the oscillations in the subdominant $\nu_e \leftrightarrow \tilde{\nu}_3$ mode are strongly enhanced by matter effects.

For $\sin^2 2\theta_{13} < 0.1$ and neutrino trajectories crossing the core of the earth the transition probability $\nu_\mu \leftrightarrow \nu_e$ as the function of energy has three peaks: two MSW peaks due to the resonance enhancement of the oscillations in the mantle and in the core and the parametric resonance peak between them. The parametric peak dominates over the MSW peaks for $\sin^2 2\theta_{13} < 0.06$.

For $\sin^2 2\theta_{13} > 0.15$ the energy intervals for the MSW resonances in the core and mantle strongly overlap and complex interference phenomena occur.

The resonance effects manifest themselves in the zenith angle dependences of the charged leptons produced in the interactions of neutrinos, although the integration over the neutrino angles and energies leads to a smearing of the zenith angle distribution of charged leptons.

We have found that the asymmetry $A_e^{U/D}(0.6, 1)$ of the multi-GeV e-like events can be as large as about 0.28 for the domain of parameters allowed by the CHOOZ bound and $s_{23}^2 = 0.75$. This value is achieved at $\Delta m_{32}^2 \simeq 10^{-3} \text{ eV}^2$ and $\sin^2 2\theta_{13} \gtrsim 0.6$. The parametric

resonance is not operative at such large values of $\sin^2 2\theta_{13}$.

The asymmetry in the parameter region $\sin^2 2\theta_{13} \lesssim 0.06$, $\Delta m_{32}^2 \approx (1 - 2) \times 10^{-3} \text{ eV}^2$ where the parametric resonance becomes important (contributes $\gtrsim 60\%$) can be as large as $A_e^{U/D}(0.6, 1) \simeq 0.22$, i.e. is close to the maximal possible value.

An important consequence of the parametric effects is that even for very small values of the mixing angle θ_{13} quite a sizeable asymmetry of the multi-GeV e-like events can result. The asymmetry can be as large as 0.15 even for $\sin^2 2\theta_{13} \simeq 0.02$.

The oscillations of the sub-GeV neutrinos could be parametrically enhanced only for about a factor of 3 smaller values of Δm_{32}^2 , close to the lower bound of the range allowed by the SK data. However even in this case the parametric resonance would not affect the asymmetries of the sub-GeV data significantly.

We have found that taking into account the subdominant $\nu_e \leftrightarrow \nu_\mu$ oscillations leads to an excess of e-likes events and improves the fit of both multi-GeV and sub-GeV e-like data in the SK experiment. However, for all allowed values of the oscillation parameters the predicted excess ($\sim 3 - 5\%$) is smaller than the observed one. Thus, if the observed excess survives future experimental tests, one will need alternative explanations for it.

The following remarks are in order.

1. If the excess of multi-GeV e-like events is at least partly due to the $\nu_e \leftrightarrow \nu_\mu$ oscillations, it leads to a lower bound on the mixing angle θ_{23} :

$$s_{23}^2 > 1/\bar{r} \simeq 0.4, \quad \text{or} \quad \theta_{23} \gtrsim 39^\circ. \quad (37)$$

This is an independent confirmation of the conclusion that ν_μ - ν_τ mixing should be rather large which follows from the data fits performed by the SK collaboration [10]. However, unlike in the SK analysis, the lower bound (37) does not depend on the μ -like data and is therefore complementary. If the excess of the sub-GeV e-like events is also at least partly due to the $\nu_e \leftrightarrow \nu_\mu$ oscillations, an even more stringent limit on θ_{23} would follow: $\theta_{23} \gtrsim 43^\circ$.

2. With increasing statistics of the SK experiment and new independent measurements

of the primary cosmic ray flux it will become possible to give a definitive answer to the question of whether there is a non-vanishing up-down asymmetry of the multi-GeV electron events beyond the small asymmetry due to the geomagnetic effects. If the answer is positive, this would be a signature of non-zero mixing θ_{13} . In a significant domain of the allowed values of Δm_{32}^2 the asymmetry is strongly enhanced by the resonance matter effects on neutrino oscillations and in particular, by the parametric resonance. This makes it possible to probe even very small values of θ_{13} in the atmospheric neutrino experiments.

The determination of the value of θ_{13} from the up-down asymmetry of the e-like events will require an independent knowledge of the values of Δm_{32}^2 and θ_{23} . These could be obtained, *e.g.*, from various samples of the μ -like events which only weakly depend on θ_{13} .

3. In principle, it is possible to experimentally disentangle the contributions from different resonance structures. Although this does not seem to be possible with the presently available data, such an analysis may become possible with future data with better statistics and/or more accurate reconstruction of neutrino energies and directions.

Clearly, selecting events in the non-vertical bins in which the trajectories that do not cross the earth's core dominate will allow one to estimate the effects of the MSW resonance in the mantle. With high statistics e-like data this can be a realistic task. Clear identification of the MSW effect on oscillations of atmospheric neutrinos in the earth would be of paramount importance.

For vertical bins one can use various energy cuts to discriminate between different resonance effects. Indeed, as we have pointed out in Sec. 3, the SK response function for multi-GeV events has a steep low-energy slope. Therefore using different energy cuts for leptons one can exclude the effects of the low energy peaks in the oscillation probability. For instance, if $\Delta m^2 \sim 2 \times 10^{-3} \text{ eV}^2$, then the response function corresponding to the threshold 1.33 GeV will cover all three resonances. However, with the threshold of 2 GeV, the effect of the parametric peak can be significantly suppressed.

4. It is interesting to note that if the preliminary BESS results [13] are confirmed and

the overall normalization of the atmospheric ν_e and ν_μ fluxes is indeed somewhat below the current theoretical predictions, the SK data would imply a smaller deficiency of atmospheric ν_μ 's. At the same time, the data on e-like events as well as the observed small value of the double ratio R would therefore mean a significant excess of the e-like events. In such a situation the excess of e-like events due to the parametric effect can be enhanced.

Indeed, a smaller deficiency of atmospheric ν_μ 's means that the value of θ_{23} , though still in a range of large mixing, may be farther away from 45° . If θ_{23} is noticeably *larger* than 45° , the excess of e-like events is further enhanced by the $(rs_{23}^2 - 1)$ factor [see (14)]. Thus, in this case of the reduced flux normalization, the parametric effects would be especially important for understanding the SK atmospheric neutrino data.

Note added :

After this work had been practically accomplished, the paper [21] has appeared in which the SK data were analyzed in the three neutrino oscillation scheme. The zenith angle distributions are shown for large θ_{13} , where parametric resonance effects play no role. The fit of the data in [21] agrees with our results: In fig. 16 of that paper, the allowed region in the triangle for $\Delta m_{32}^2 = 10^{-3} \text{ eV}^2$ corresponds to $s_{23}^2 > 0.5$ and small nonzero θ_{13} .

Acknowledgments

We would like to thank Eligio Lisi for useful discussions. One of us (PL) wishes to thank Serguey Petcov for discussions on similar ideas about three flavor oscillations in atmospheric neutrinos.

Appendix : Cross-sections and event rates

To describe the neutrino cross section we have considered separately the processes of quasi-elastic scattering, single pion production and multi-particle production [22]. We have also included nuclear effects according to the treatment of Smith and Moniz [23] - the nucleons bound in the oxygen nucleus were assumed to fill a Fermi sphere up to a maximum momentum $p_F = 220$ MeV, and to have a binding energy of 25 MeV.

The quasi elastic scattering was described following Llewellyn Smith [24], using $F_A(Q^2) = -1.25(1 + Q^2/M_A^2)^{-2}$ for the axial-vector form factor, with $M_A = 1.0$ GeV [25]. The nuclear effects are important for the quasi-elastic cross section: the processes where the final state nucleon is scattered in an occupied state are prohibited by the Pauli blocking effect and the cross section is reduced. The Fermi momentum of the bound nucleons also has the effect of broadening the angular distribution of the final state charged leptons.

The cross section for the single pion production in the region $W < 1.4$ GeV (W is the mass of the hadronic system in the final state) was described following Fogli and Nardulli [26]. In this region the most important dynamical effect is the presence of the Δ resonance.

All the other scattering processes were described using the standard formula for deep inelastic scattering using the leading order parton distribution functions (PDF's) of Gluck, Reya and Vogt [27]. In the monte carlo calculation we used the LUND algorithms [28, 29] to construct physical particles from the hadronic state composed of the scattered (anti-)quarks and the nucleon remnants were described [30] as a qq , $qqqq$ or $qqq\bar{q}$ system.

We have used a monte carlo method for the calculation. This allows to include all the dynamical features in detail, including the important nuclear effects, and also to simulate (at least crudely) the experimental selection criteria (in particular the 'single-ring' and containment conditions). Our monte carlo also generated neutral-current events, but we have not considered the possibility of the mis-classification of NC events as CC events.

To simulate single-ring events we selected the events with a charged lepton in the appro-

priate range of momentum, and required in addition the absence of photons or additional charged particles above the Cherenkov threshold. The single ring requirement is important because it preferentially selects lower energy neutrinos and therefore changes the response function for the different categories of events. For the containment requirement, we assumed that all electron events in the fiducial volume were contained; for each muon event generated a neutrino interaction point in the fiducial volume and checked whether the range in water of the final state μ^\pm was shorter or longer than the distance along the trajectory from the interaction point to the PMT surface.

Our no-oscillation calculation is approximately 20% lower in normalization than the Super-Kamiokande monte carlo for all five categories of events (e-like and μ -like sub-GeV and multi-GeV fully contained events and partially contained events), with very good agreement in the zenith angle distributions. The absolute normalization of the calculation is sensitive to details such as the minimum amount of Cherenkov light that a charged particle needs to have in order to produce an additional visible ring. For the purposes of our discussion we find the agreement to be good.

References

- [1] V. K. Ermilova, V. A. Tsarev and V. A. Chechin, Kr. Soob, Fiz. [Short Notices of the Lebedev Institute] **5**, 26 (1986).
- [2] E. Kh. Akhmedov, preprint IAE-4470/1, (1987); Yad. Fiz. **47**, 475 (1988) [Sov. J. Nucl. Phys. **47**, 301 (1988)].
- [3] P. I. Krastev and A. Yu. Smirnov, Phys. Lett. B **226**, 341 (1989).
- [4] Q. Y. Liu and A. Yu. Smirnov, Nucl. Phys. B524 (1998) 505, hep-ph/9712493; Q. Y. Liu, S. P. Mikheyev and A. Yu. Smirnov, hep-ph/9803415.
- [5] P. Lipari and M. Lusignoli, hep-ph/9803440.

- [6] S. T. Petcov, preprint SISSA 31/98/EP, hep-ph/9805262.
- [7] E. Kh. Akhmedov, hep-ph/9805272.
- [8] E. D. Carlson, Phys. Rev D **34**, 1454 (1986); A. Dar, A. Mann, Y. Melina, and D. Zajfman, Phys. Rev. D **35**, 3607 (1988); G. Auriemma, M. Felcini, P. Lipari and J. L. Stone, Phys. Rev. D **37**, 665 (1988).
- [9] A. J. Baltz and J. Weneser, Phys. Rev. D **35**, 528 (1987); M. Cribier, W. Hampel, J. Rich, and D. Vignaud, Phys. Lett. B **182**, 89 (1986); A. Dar *et al.*, ref. [8]; A. Nicolaidis, Phys. Lett. B **200**, 553 (1988); P. I. Krastev and S. P. Petcov, Phys. Lett. **B205**, 84 (1988); J. M. LoSecco, Phys. Rev. D **47**, 2032 (1993); J. M. Gelb, W.-K. Kwong, and S. P. Rosen, Phys. Rev. Lett. **78**, 2296 (1997); Q. Y. Liu, M. Maris and S. T. Petcov, Phys. Rev. D **56**, 5991 (1997); M. Maris and S. T. Petcov, Phys. Rev. D **56**, 7444 (1997); M. Maris and S. T. Petcov, hep-ph/9803244.
- [10] Super-Kamiokande Collaboration, Y. Fukuda *et al.*, hep-ex/9803006; hep-ex/9805006; hep-ex/9807003; T. Kajita, Talk at the International Conference on Neutrino Physics and Astrophysics “*Neutrino’98*”, Takajama, Japan, June 1998.
- [11] Kamiokande collaboration, K.S. Hirata *et al.*, Phys. Lett. B **280**, 146 (1992); Y. Fukuda *et al.*, Phys. Lett. B **335**, 237 (1994); IMB collaboration, R. Becker-Szendy *et al.*, Nucl. Phys. Proc. Suppl. **38B**, 331 (1995); Soudan-2 collaboration, W.W.M. Allison *et al.*, Phys. Lett. B **391**, 491 (1997).
- [12] CHOOZ collaboration, M. Apollonio *et al.*, Phys.Lett. B **420**, 397 (1998) (hep-ex/9711002).
- [13] T. Sanuki, Talk at the Symposium “*New Era in Neutrino Physics*” (Satellite Symposium after “*Neutrino’98*”), Tokyo, June 1998.
- [14] J. M. LoSecco, hep-ph/9807359.

- [15] J. Pantaleone, Phys. Rev. D **49**, 2152 (1994); G. L. Fogli, E. Lisi, D. Montanino, Astropart. Phys. **4**, 177 (1995); G. L. Fogli, E. Lisi, D. Montanino, G. Scioscia, Phys. Rev. D **55**, 4385 (1997); G. L. Fogli, E. Lisi, A. Marrone, Phys. Rev. D **57**, 5893 (1998); O. Yasuda, hep-ph/9706546; hep-ph/9804400.
- [16] C. Giunti, C. W. Kim, J. D. Kim, Phys. Lett. B **352**, 357 (1995); P. F. Harrison, D. H. Perkins, Phys. Lett. B **349**, 137 (1995); Phys. Lett. B **396**, 186 (1997); H. Fritzsch, Z.-Z. Xing, Phys. Lett. B **372**, 265 (1996); C. Giunti, C. W. Kim, M. Monteno, Nucl. Phys. B **521**, 3 (1998); R. Foot, R. R. Volkas, O. Yasuda, Phys. Lett. B **421**, 245 (1998) (hep-ph/9710403); hep-ph/9802287.
- [17] G. L. Fogli, E. Lisi, A. Marrone, D. Montanino, Phys. Lett. B **425**, 341 (1998).
- [18] G. L. Fogli, E. Lisi, D. Montanino, Phys. Rev. D **49**, 3626 (1994); G. L. Fogli, E. Lisi, G. Scioscia, Phys. Rev. D **52**, 5334 (1995); S. M. Bilenkii, C. Giunti, C. W. Kim, Astropart. Phys. **4**, 241 (1996); O. Yasuda, H. Minakata, hep-ph/9602386; Nucl.Phys.B **523**, 597 (1998) (hep-ph/9712291); T. Teshima, T. Sakai, O. Inagaki, hep-ph/9801276; T. Teshima, T. Sakai, hep-ph/9805386; V. Barger, S. Pakvasa, T. J. Weiler, K. Whisnant, hep-ph/9806387; R. Barbieri, L. J. Hall, D. Smith, A. Strumia, N. Weiner, hep-ph/9807235; V. Barger, T. J. Weiler, K. Whisnant, hep-ph/9807319.
- [19] F.D. Stacey, *Physics of the Earth*, John Wiley and Sons, New York, 1969.
- [20] KAMLAND Project, P. Alivisatos *et al.*, preprint Stanford-HEP-98-03, Tohoku-RCNS-98-03.
- [21] G. L. Fogli, E. Lisi, A. Marrone and G. Scioscia, BARI-TH/309-98, hep-ph/9808205.
- [22] P. Lipari, M. Lusignoli, and F. Sartogo, Phys. Rev. Lett. **74**, 4384 (1995).
- [23] R.A. Smith and E.J. Moniz, Nucl. Phys. B **43**, 605, (1972).
- [24] C.H. Llewellyn Smith, Phys.Rep. **3**, 271 (1971).

- [25] S.V. Belikov, Z.Phys.A **320**, 625 (1985).
- [26] G.L. Fogli and G. Nardulli, Nucl.Phys.B **160**, 116 (1979).
- [27] M. Gluck, E. Reya, and A. Vogt, Z.Phys. C **67**, 433 (1995).
- [28] B. Andersson, G. Gustafson, G. Ingelman, T. Sjöstrand, Phys. Rep. **97**, 31 (1983).
- [29] T. Sjöstrand, JETSET version 7.4, preprint hep-ph/9508391 (1995).
- [30] G. Ingelman et al., in Proc. of the HERA Workshop 1987, Ed. R.D. Peccei, DESY Hamburg 1988 Vol. 1, p. 3, (1988). G. Ingelman, LEPTO version 5.2, unpublished program manual.

Figure captions

Fig. 1. Dependence of the transition probability P_2 on neutrino energy for $\Delta m_{32}^2 = 2 \times 10^{-3}$ eV² (a) for $\sin^2 2\theta_{13} = 0.025$ and different values of $\cos \Theta_\nu$: -0.98 (solid curve), -0.88 (long-dashed curve), and -0.85 (short-dashed curve); (b) for $\cos \Theta_\nu = -0.98$ and different values of $\sin^2 2\theta_{13}$: 0.014 (short-dashed curve), 0.025 (long-dashed curve), 0.057 (solid curve). Neutrino energy in eV.

Fig. 2. Zenith angle dependences of multi-GeV events. (a) e-like events: solid line – no oscillations, dashed line corresponds to oscillations with $\sin^2 2\theta_{13} = 0.06$, $\sin^2 \theta_{23} = 0.75$ and $\Delta m_{32}^2 = 10^{-3}$ eV². (b) μ -like events: upper solid histogram is for no-oscillations case, the dashed histogram – oscillations with $\sin^2 2\theta_{13} = 0.06$, $\sin^2 \theta_{23} = 0.75$ and $\Delta m_{32}^2 = 10^{-3}$ eV², the lower solid histogram – two-neutrino oscillations with the same parameters but $\sin^2 2\theta_{13} = 0$.

Fig. 3. Dependence of the up-down asymmetries of multi-GeV (a) e-like events, $A_e^{U/D}(0.6, 1)$, and (b) μ -like events, $A_\mu^{U/D}(0.6, 1)$, on Δm_{32}^2 for $s_{23}^2 = 0.75$ and different values of $\sin^2 2\theta_{13}$: $\sin^2 2\theta_{13} = 0.03$ (dashed curve), 0.06 (solid curve), 0.10 (dot - dashed) curve. The dotted curve in fig. 3b shows the asymmetry for pure $\nu_\mu \leftrightarrow \nu_\tau$ oscillations with $s_{23}^2 = 0.75$. (c). The same as in fig. 3a but for different bins: $A_e^{U/D}(0.84, 1)$ (dashed curve), $A_e^{U/D}(0.60, 0.84)$ (dot-dashed curve) and $A_e^{U/D}(0.60, 1)$ (solid curve); $\sin^2 2\theta_{13} = 0.06$.

Fig. 4. Dependence of the up-down asymmetries of multi-GeV (a) e-like events, $A_e^{U/D}(0.6, 1)$, and (b) μ -like events, $A_\mu^{U/D}(0.6, 1)$, on $\sin^2 2\theta_{13}$ for $s_{23}^2 = 0.75$ and different values of Δm_{32}^2 : 0.5×10^{-3} eV² (dot-dashed curve), 1.7×10^{-3} eV² (dashed curve), 3×10^{-3} eV² (solid curve). The squares on the curves represent the CHOOZ bound: parts of the curves on the right of the squares are excluded.

Fig. 5. Dependence of the up-down asymmetries (a) of e-like events, $A_e^{U/D}(0.6, 1)$, and (b) of μ -like events, $A_\mu^{U/D}(0.6, 1)$, on s_{23}^2 for $\Delta m_{32}^2 = 1.7 \times 10^{-3}$ eV² and different values of $\sin^2 2\theta_{13}$: $\sin^2 2\theta_{13} = 0.03$ (dashed curve), 0.06 (solid curve), 0.10 (dot - dashed curve). The

dotted curve in fig. 5b shows the asymmetry for pure $\nu_\mu \leftrightarrow \nu_\tau$ oscillations with $s_{23}^2 = 0.75$.

Fig. 6. Zenith angle dependence of the multi-GeV e-like events. The solid histogram is for the no-oscillation case. The dashed histogram is calculated for $\Delta m^2 = 1.7 \times 10^{-3} \text{ eV}^2$, $\sin^2 2\theta_{13} = 0.10$ and $\sin^2 2\theta_{23} = 0.75$. The points are the 535 days data of the Super-Kamiokande.

Fig. 7. Iso-asymmetry contour plot for multi-GeV e-like events in the $(\sin^2 2\theta_{13}, \Delta m_{32}^2)$ plane for $s_{23}^2 = 0.75$. The closed curve corresponds to $A_e^{U/D} = 0.264$. The other curves (from bottom upward): $A_e^{U/D} = 0.15, 0.175, 0.20, 0.225, 0.25, 0.275, 0.30, 0.325, 0.35, 0.375, 0.40, 0.425$ and 0.45 . The shaded area shows the region excluded by CHOOZ.

Fig. 8. Zenith angle distribution of the e-like events in the sub-GeV range. Solid histogram – without oscillations; dashed histogram – oscillations with $\Delta m_{32}^2 = 0.3 \times 10^{-3} \text{ eV}^2$, $\sin^2 2\theta_{13} = 0.1$ and $\sin^2 \theta_{23} = 0.75$. The points are the 535 days data of the Super-Kamiokande.

Fig. 9. (a) The ratio of the e-like events rates in the sub-GeV region with and without oscillations as the function of Δm_{32}^2 for $\sin^2 \theta_{23} = 0.75$ (solid curves) and $\sin^2 \theta_{23} = 0.65$ (dashed curves) and different values of $\sin^2 2\theta_{13}$. From the lowest to the highest curve: $\sin^2 2\theta_{13} = 0.03, 0.06, 0.10, 0.20$. (b) the same as in fig. 7a but for μ -like events. $\sin^2 2\theta_{13} = 0.03, 0.06, 0.10, 0.20$ (from the highest to the lowest curve). The dotted curve corresponds to pure $\nu_\mu \leftrightarrow \nu_\tau$ oscillations with $\sin^2 \theta_{23} = 0.5$.

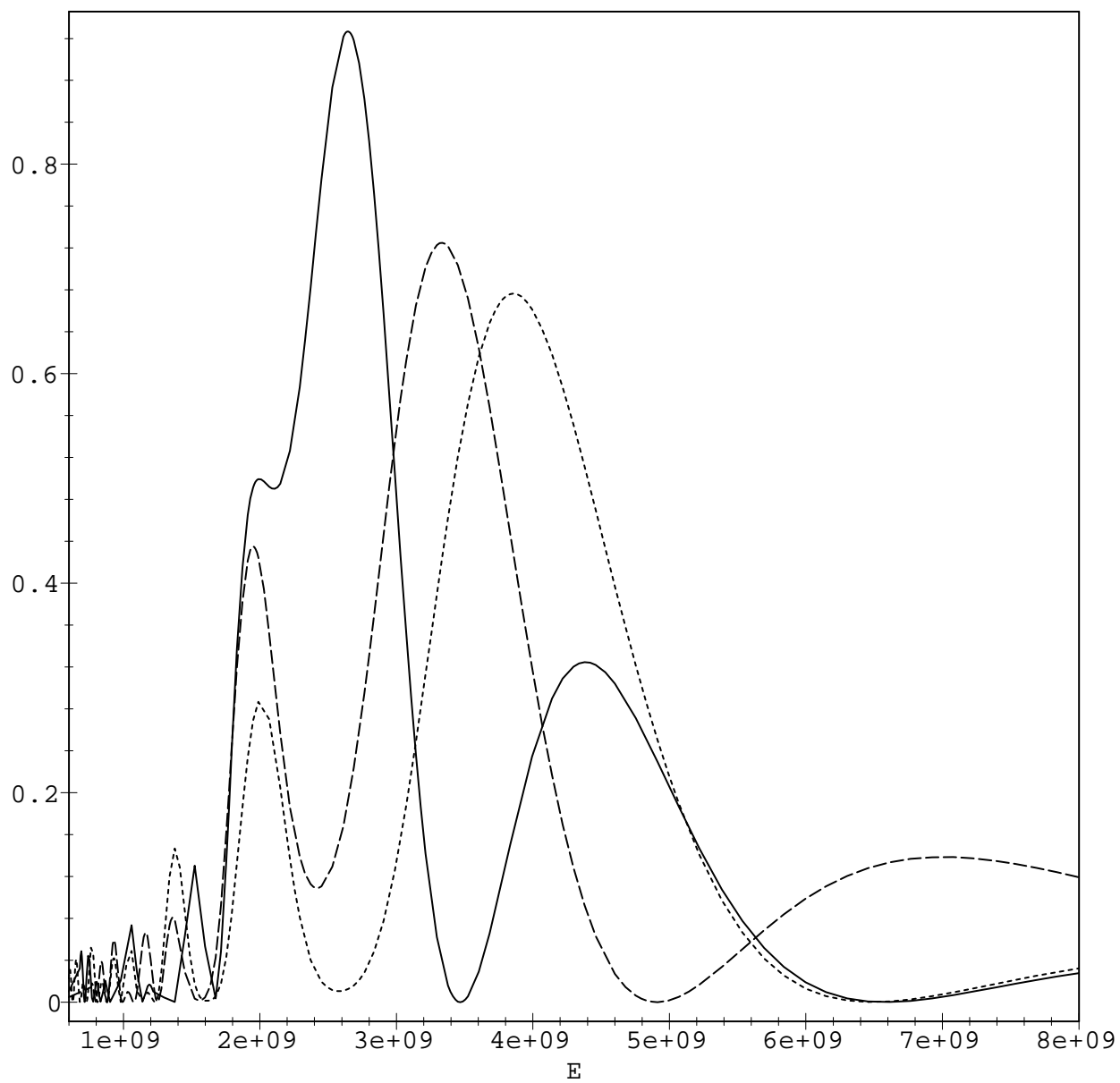


Figure 1a

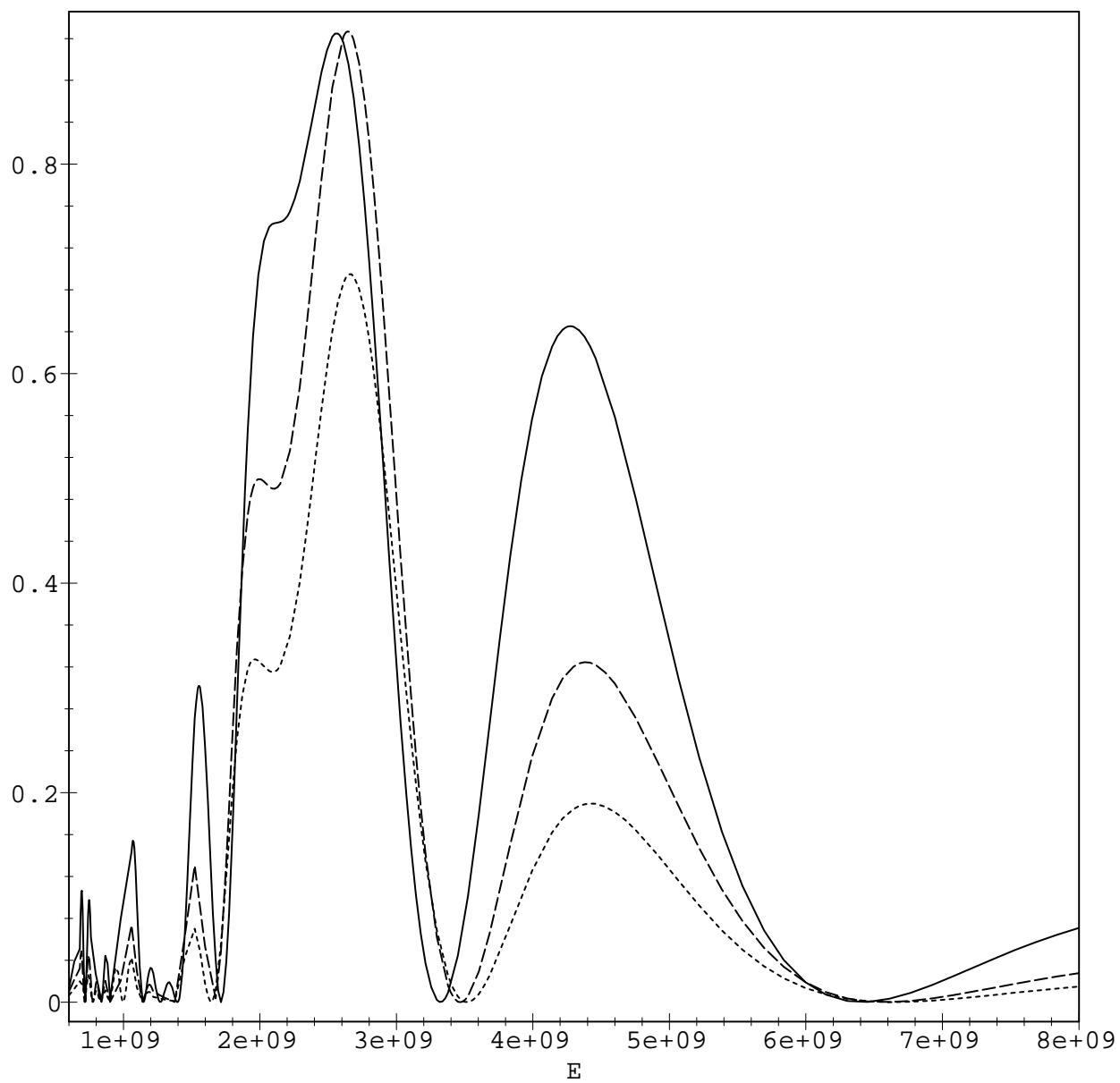


Figure 1b

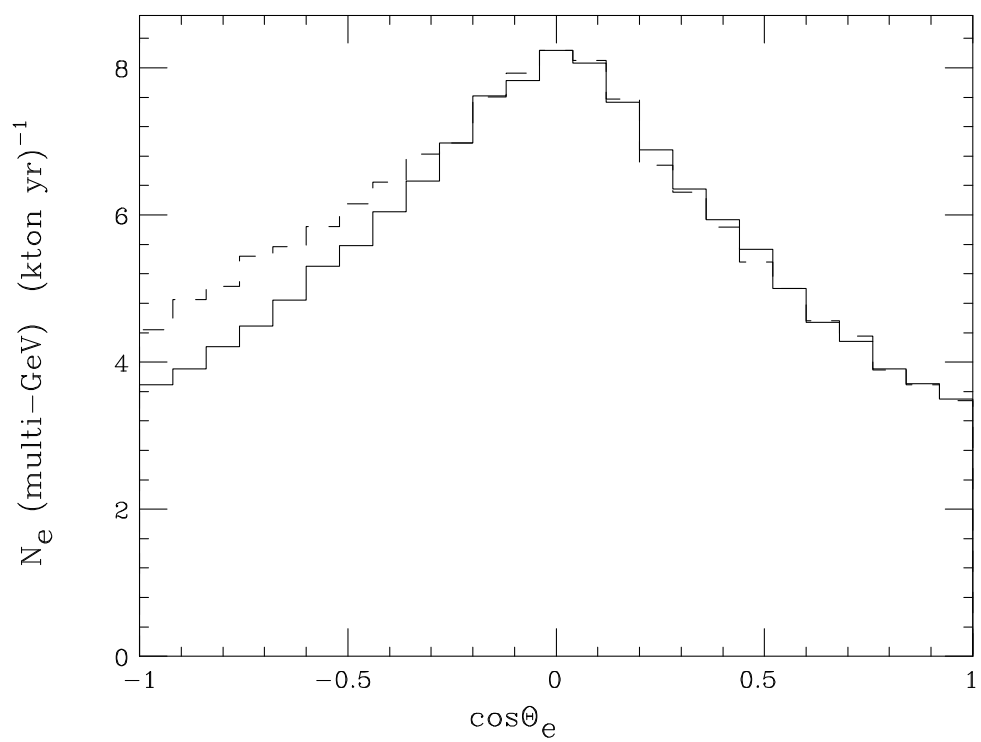


Figure 2a

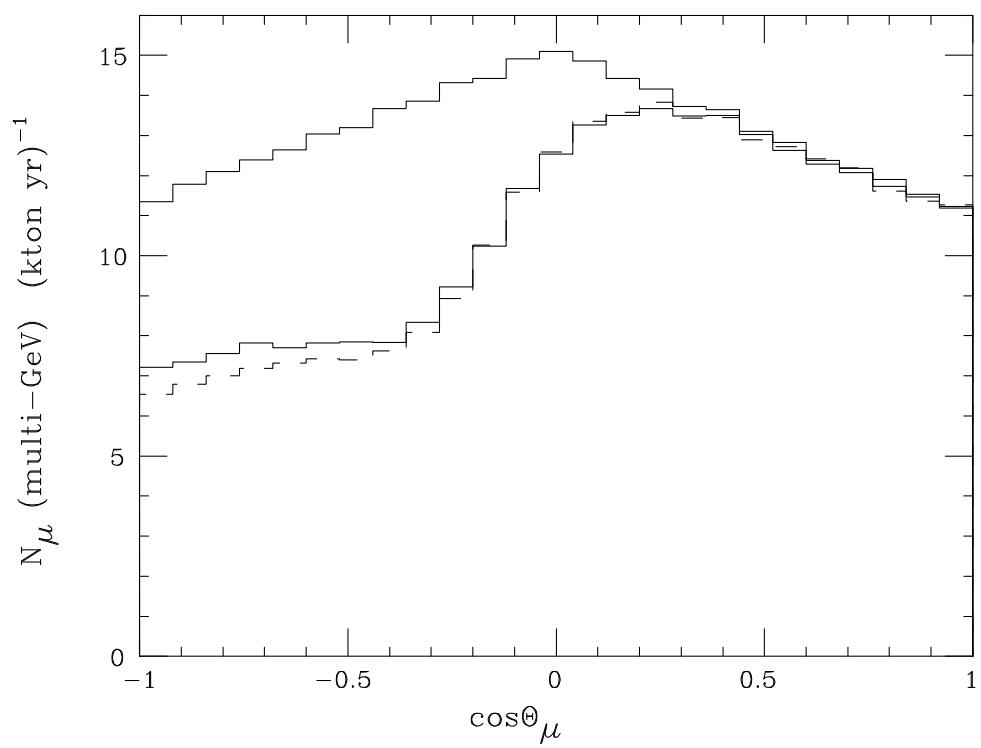


Figure 2b

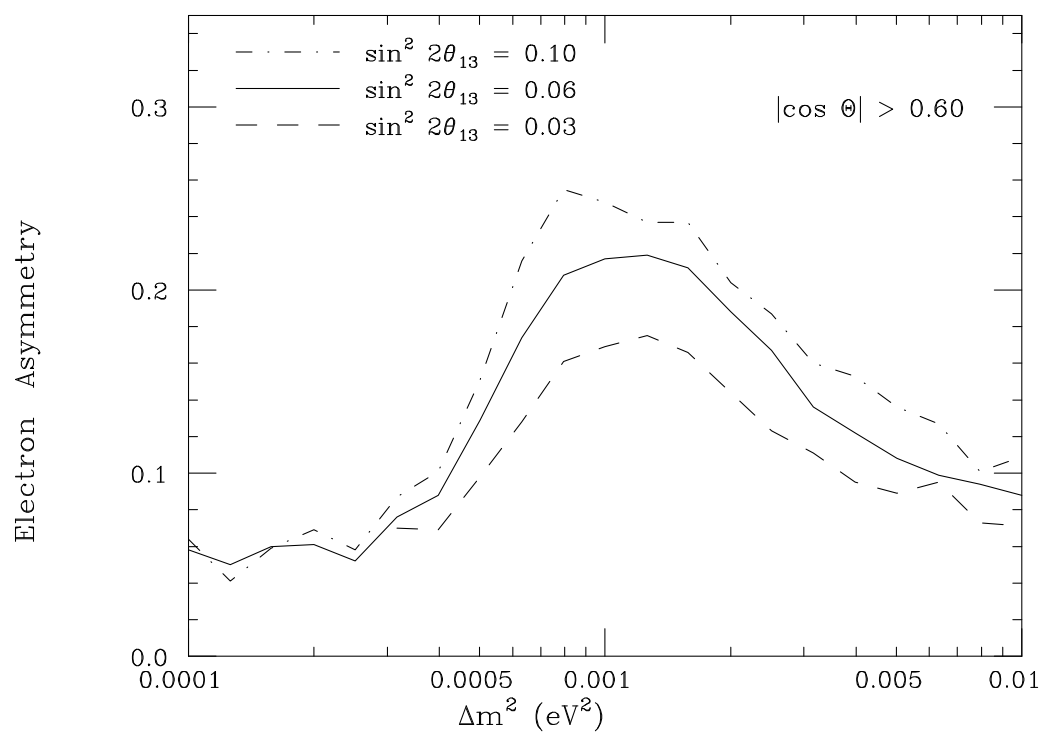


Figure 3a

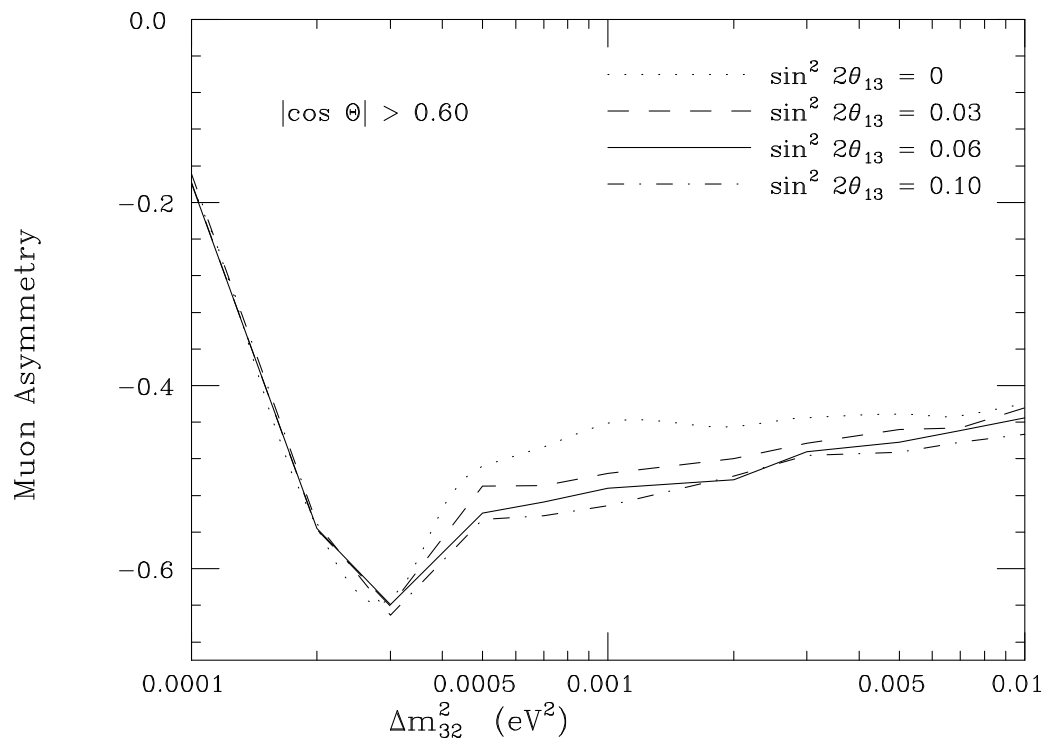


Figure 3b

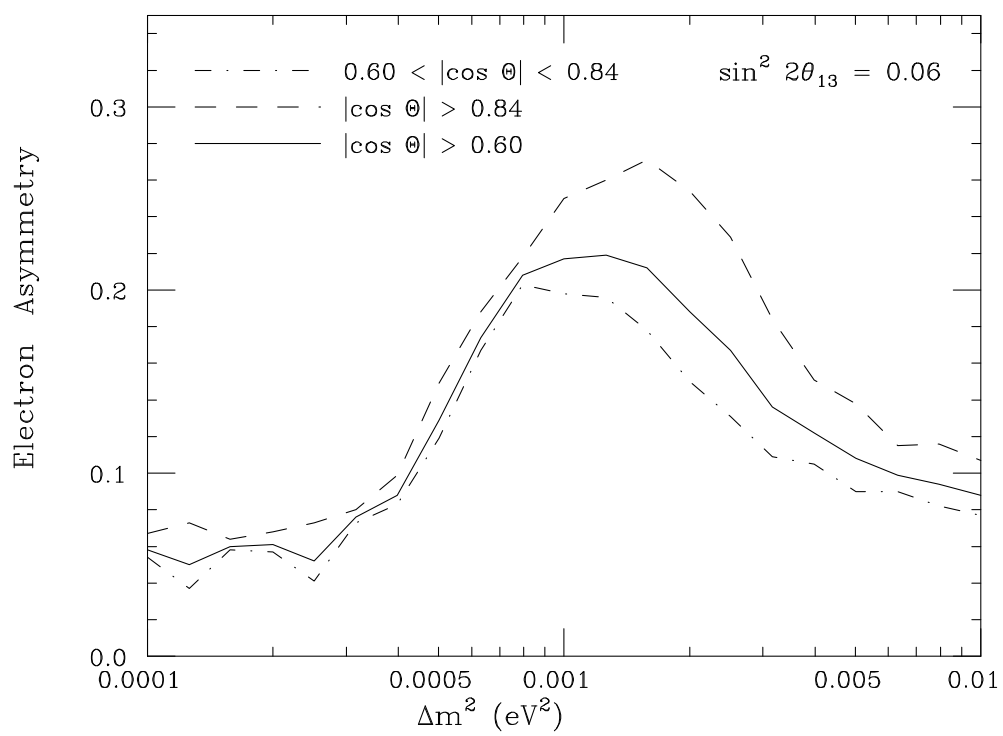


Figure 3c

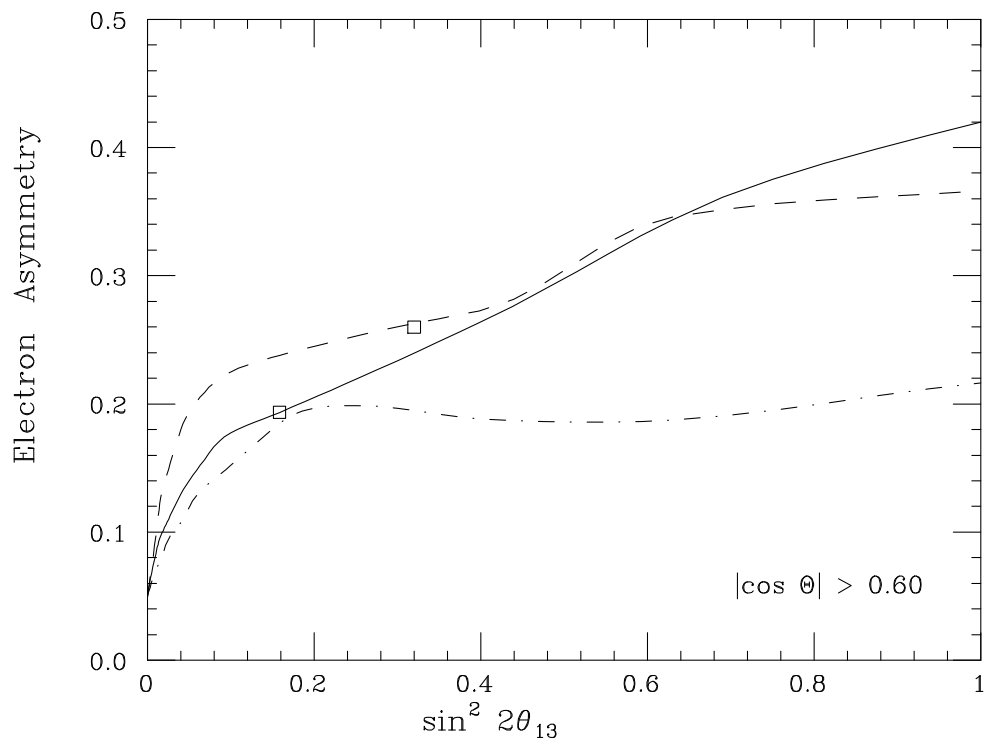


Figure 4a

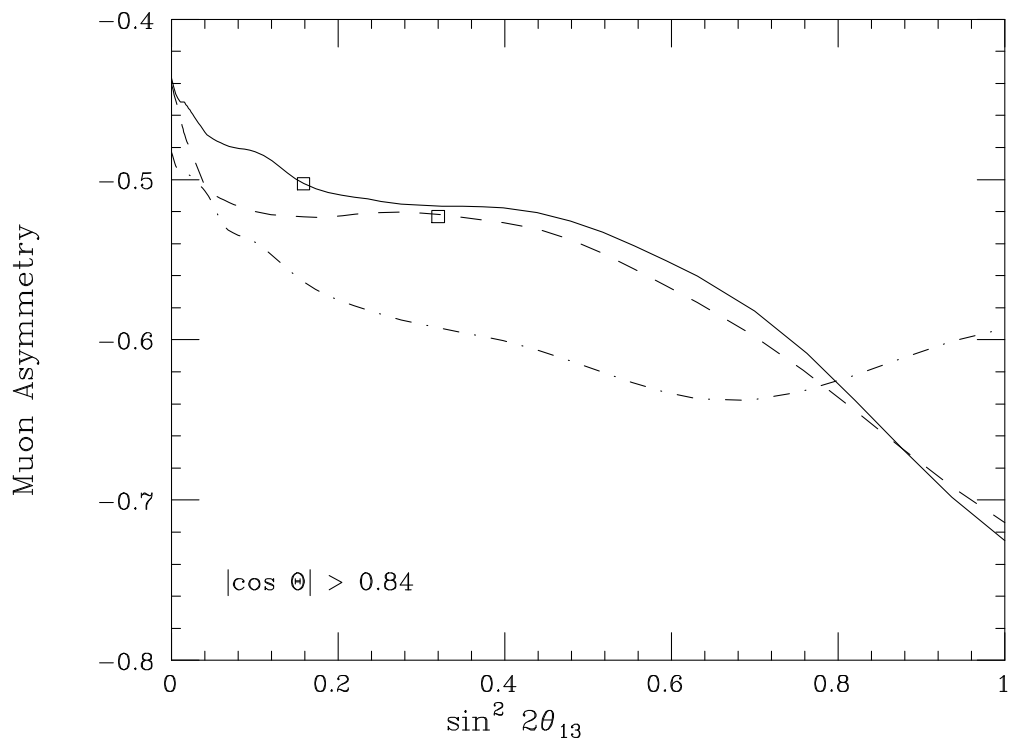


Figure 4b

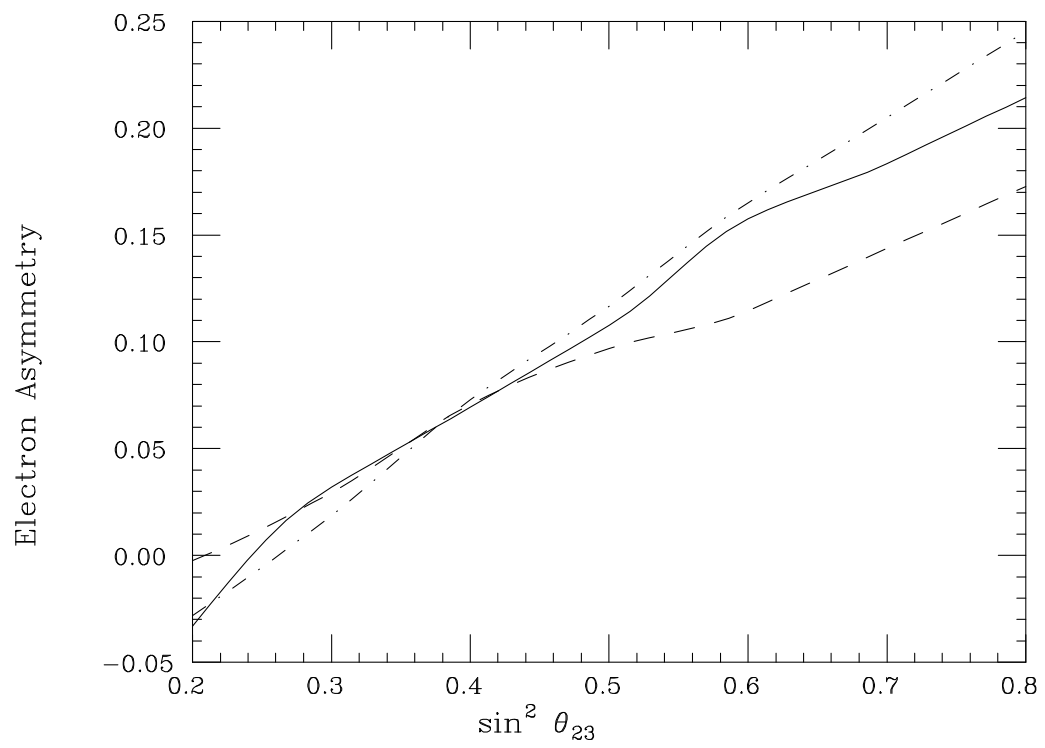


Figure 5a

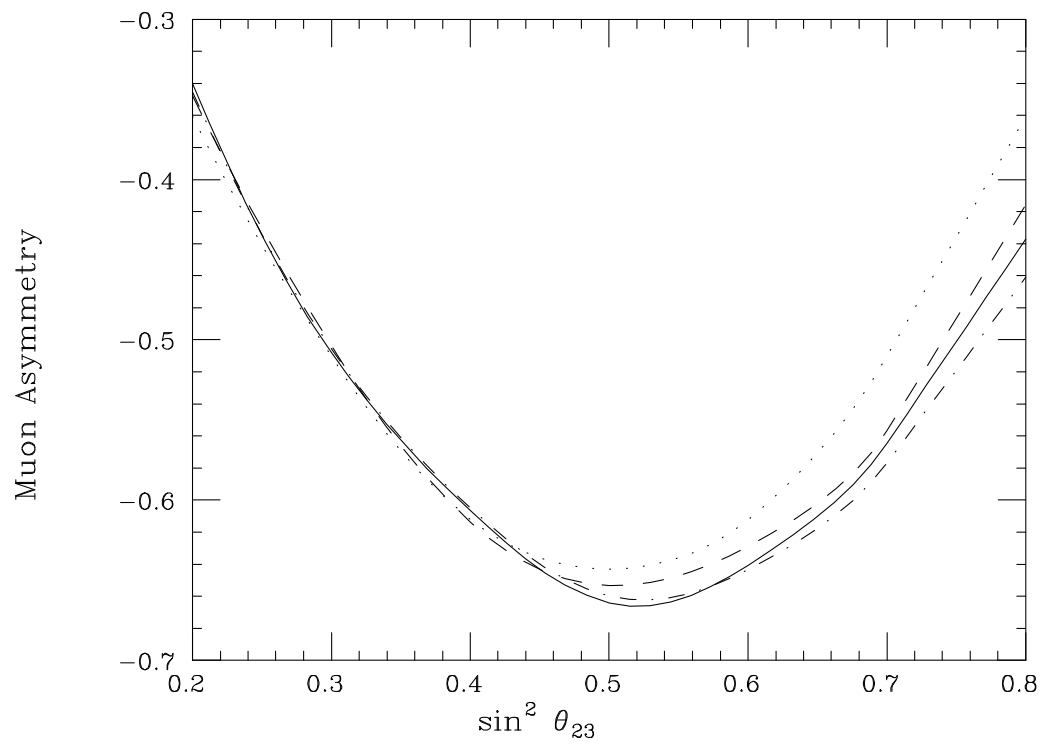


Figure 5b

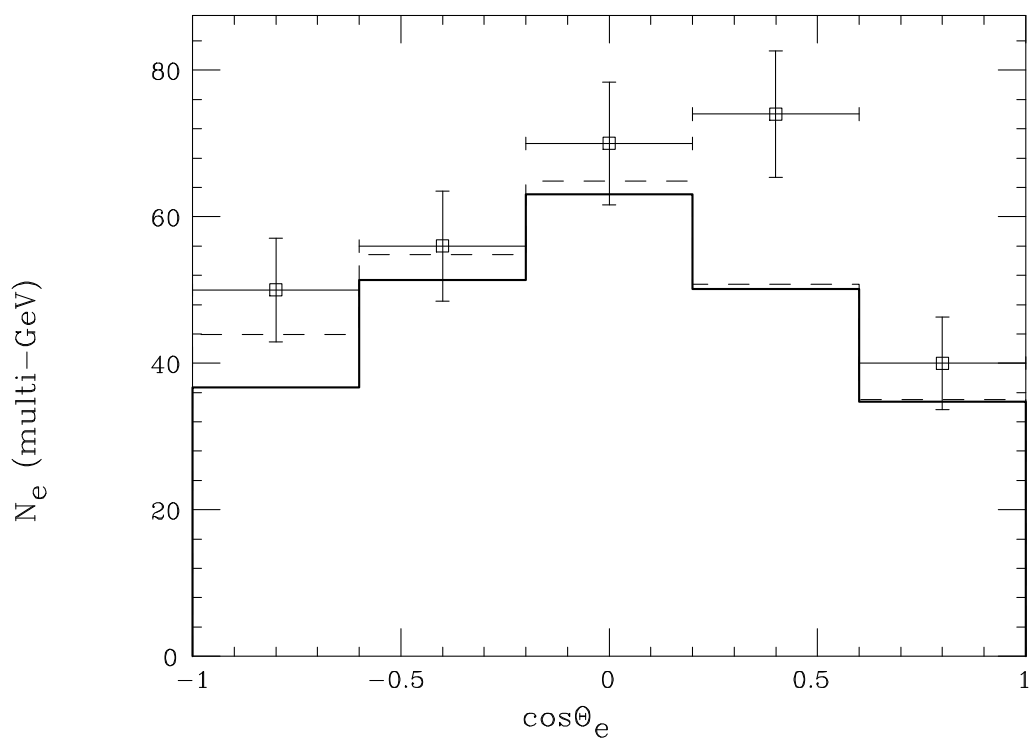


Figure 6

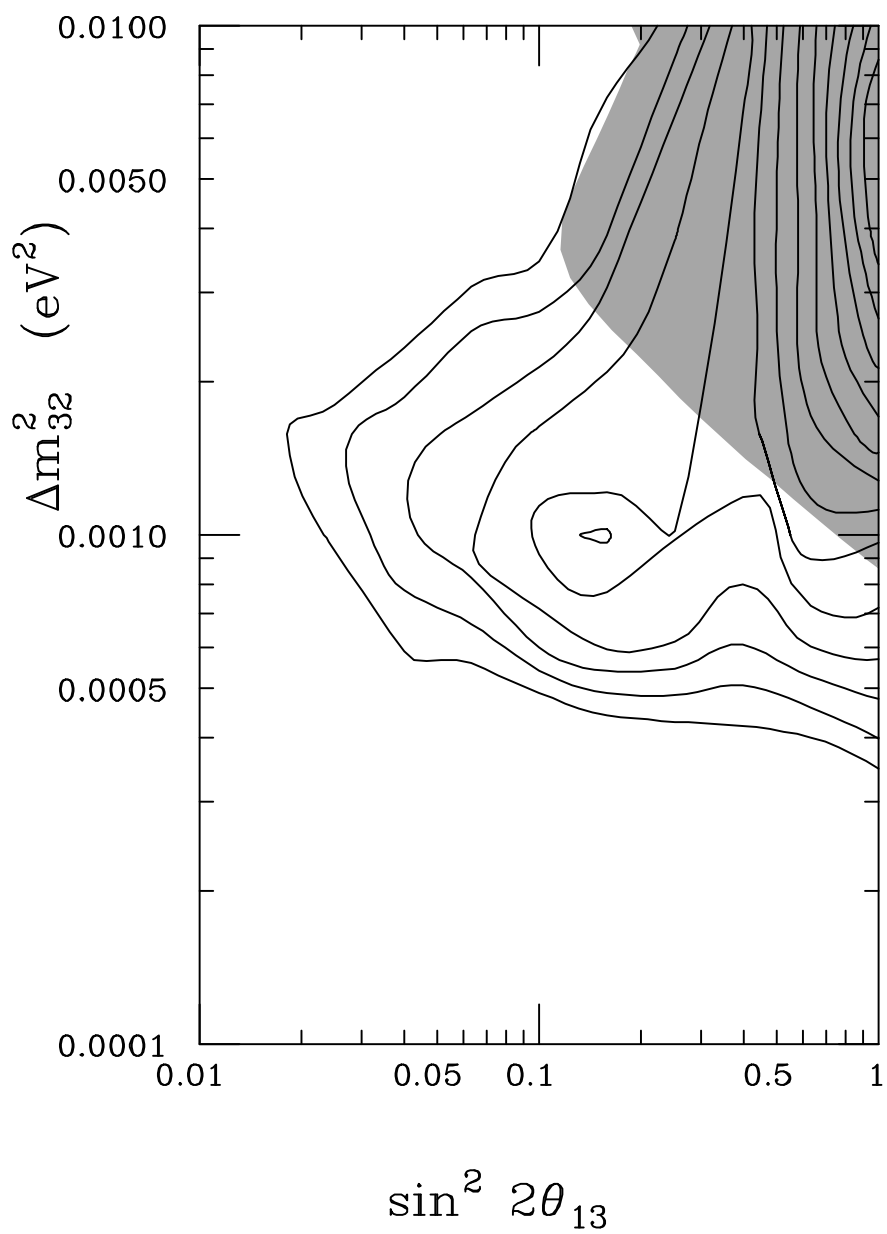


Figure 7

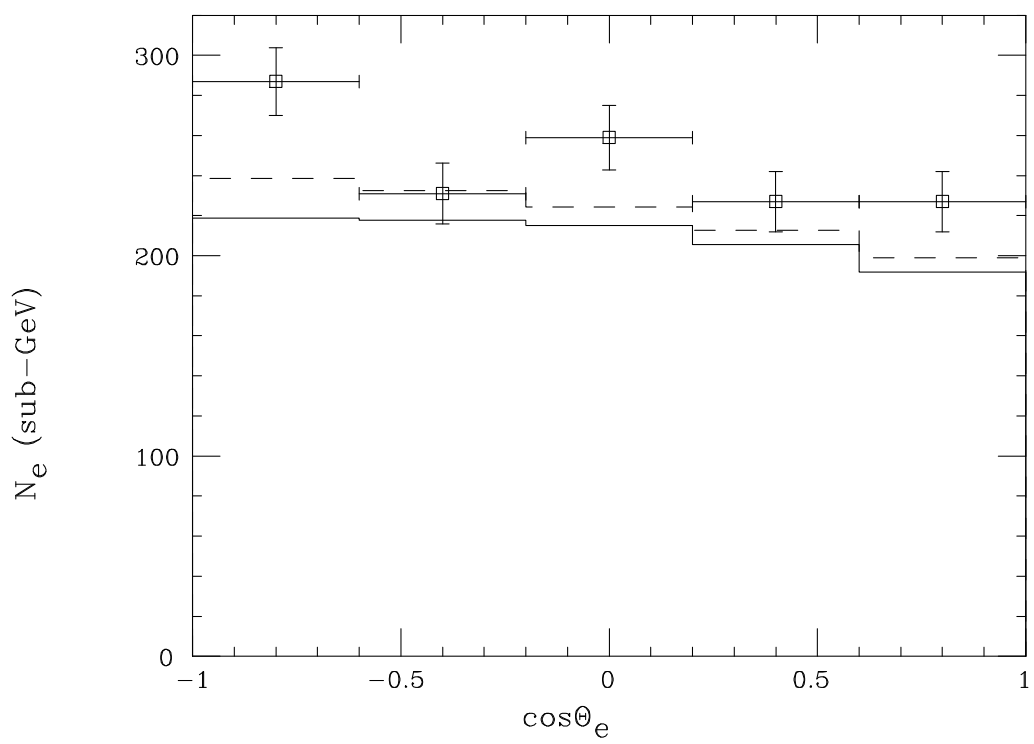


Figure 8

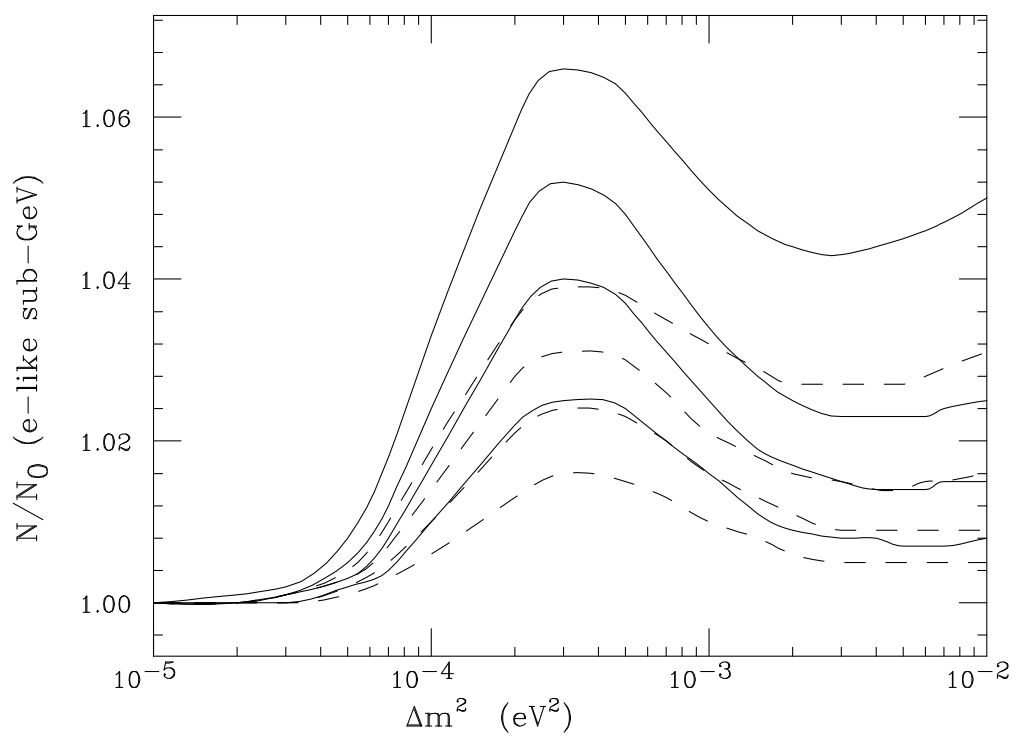


Figure 9a

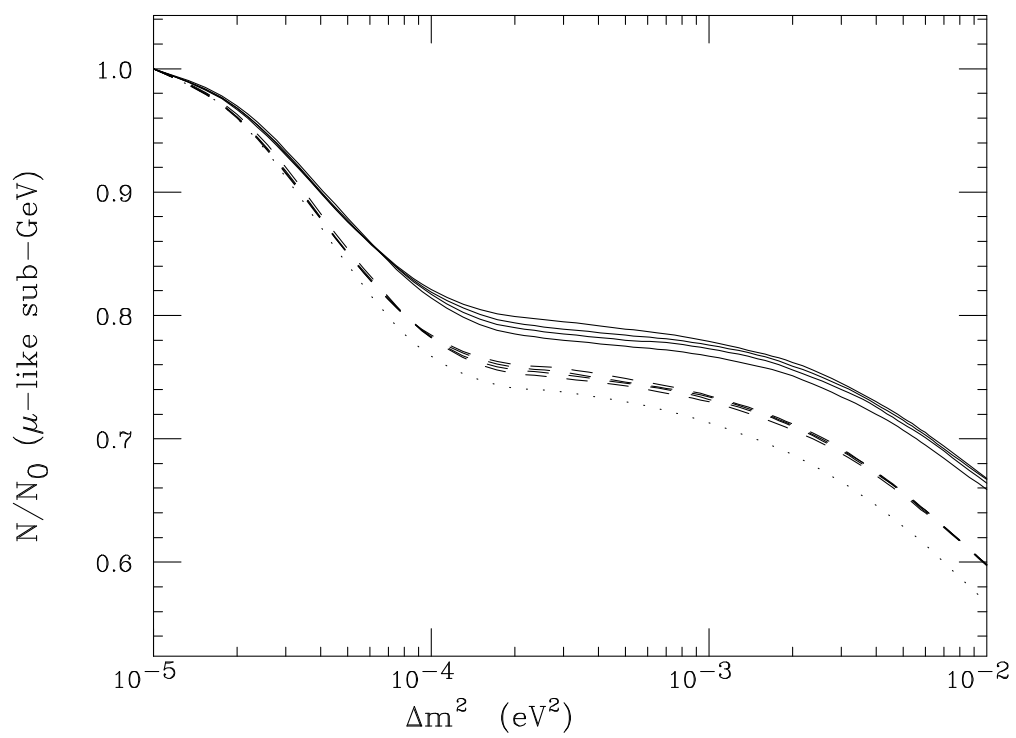


Figure 9b